Title

Moniliform deformation of retinal ganglion cells by formaldehyde-based fixatives

Journal

The Journal of Comparative Neurology, 523(4)

ISSN

1550-7149

Authors

Stradleigh, Tyler W
Greenberg, Kenneth P
Partida, Gloria J
et al.

Publication Date

2015-03-01

DOI

10.1002/cne.23689

Peer reviewed

Published in final edited form as:
J Comp Neurol. 2015 March 1; 523(4): 545–564. doi:10.1002/cne.23689.

Moniliform Deformation of Retinal Ganglion Cells by Formaldehyde-Based Fixatives

Tyler W. Stradleigh[1], **Kenneth P. Greenberg**[2,3], **Gloria J. Partida**[1], **Aaron Pham**[2], and **Andrew T. Ishida**[1,4]

[1]Department of Neurobiology, Physiology and Behavior, University of California, Davis, CA 95616

[2]Department of Molecular and Cell Biology, University of California, Berkeley, CA 94720

[3]EOS Neuroscience, Inc., San Francisco, CA 94103

[4]Department of Ophthalmology and Vision Science, University of California, Sacramento, CA 95817

Abstract

Protocols for characterizing cellular phenotypes commonly use chemical fixatives to preserve anatomical features, mechanically stabilize tissue, and stop physiological responses. Formaldehyde, diluted in either phosphate-buffered saline or phosphate buffer, has been widely used in studies of neurons, especially in conjunction with dyes and antibodies. However, previous studies have reported that these fixatives induce the formation of bead-like varicosities in the dendrites and axons of brain and spinal cord neurons. We report here that these formaldehyde formulations can induce bead formation in the dendrites and axons of adult rat and rabbit retinal ganglion cells, and that retinal ganglion cells differ from hippocampal, cortical, cerebellar, and spinal cord neurons in that bead formation is not blocked by glutamate receptor antagonists, a voltage-gated Na^+ channel toxin, extracellular Ca^{2+} ion exclusion, or temperature shifts. Moreover, we describe a modification of formaldehyde-based fixatives that prevents bead formation in retinal ganglion cells visualized by green fluorescent protein expression and by immunohistochemistry.

Keywords

paraformaldehyde; varicosities; sucrose; dendrites; axons; retina; RRID:RGD_60991 (organism_LErat); RRID:AB_10058149 (antibody_GFP); RRID:AB_2156044 (antibody_melanopsin); RRID:AB_1566483 (antibody_SMI32); RRID:AB_10562716 (antibody_DKaRBaf555); RRID:AB_10049285 (antibody_DKaMSaf488); RRID:NIF-0000-30467(software_ImageJ); RRID:NLX_143660 (database_JCNantibody)

*Corresponding author: Andrew Ishida, Department of Neurobiology, Physiology and Behavior, University of California, One Shields Avenue, Davis, CA 95616-8519, tel: (530) 752-3569, fax: (530) 752-5582, atishida@ucdavis.edu.

Associate Editor: Ian A. Meinertzhagen

CONFLICT OF INTEREST: The authors declare no competing financial interests.

ROLE OF AUTHORS: All authors had full access to all the data in the study and take responsibility for the integrity of the data and the accuracy of the data analysis. Study concept and design: ATI, TWS, KPG, GJP. Acquisition of data: TWS, KPG, ATI. Analysis and interpretation of data: TWS, ATI. Drafting of the manuscript: ATI, TWS. Technical support: AP, GJP.

INTRODUCTION

Chemical fixatives are commonly used to preserve anatomical features in studies of cell types, dimensions, interconnections, immunoreactivities, stages of development, and impacts of disease (Fox et al., 1985; Cohen and Sterling, 1990; Marc et al., 1995; Micheva and Smith, 2007; Boon and Kok, 2008; Anderson et al., 2009). Few tissues are more exacting to fix than vertebrate retinae because they are delicate and contain 50–120 cell types (Ramón y Cajal, 1893; Marc, 2008). Moreover, the morphology of even healthy adult retinal neurons can change under physiological conditions (Arey, 1915; Schaeffer and Raviola, 1978; Behrens et al., 1998). For more than 40 years, and in several protocols devised to identify cells (Nelson, 1977; Stewart, 1978; Tauchi and Masland, 1984; Vaney, 1991; Fernandez and Kolb, 1993; Bhide et al., 1994; Pow et al., 1995; Zhan and Troy, 1997; Rivera and Lugo, 1998; Hattar et al., 2002; Sun et al., 2002; Dacey et al., 2003; Kong et al., 2005; Hoshi et al., 2006; Sarthy et al., 2007; Kim et al., 2008; Raymond et al., 2008; Kanjhan and Vaney, 2008; Siegert et al., 2009), it has been widespread practice to immerse isolated retinae, hemisected eyecups, and whole eyes in formaldehyde-based fixatives (abbreviated hereafter as FA). While it is possible that retinal neurons are anatomically "correct" in FA-fixed preparations, at least two challenges are encountered following immersion in FA.

One is that tissue is susceptible to shrinkage during dehydration, defatting, and mounting (Grace and Llinás 1985; Bucher et al., 2000). This change may be refractory to *post hoc* correction because it can be greater in some cell layers than others (Anger et al., 2004) and greater in one axis than others (Trommald et al., 1995; Gardella et al., 2003). A second hurdle is to preserve the shape of dendrites and axons. Although it is possible that the diameter and contour of these neurites are not altered by fixation, micrographs of many aldehyde-fixed retinal ganglion cells show moniliform swellings (e.g., Stanford and Sherman, 1984; Huxlin and Goodchild, 1997). These swellings are typically round, uniformly-sized, not more than a few μm in diameter, and separated by segments of small-caliber neurites. Each swelling of this type is often referred to as a "bead" because lines of these resemble strings of beads (Ramón y Cajal, 1899; Price and Powell, 1970). Some studies have interpreted beads as part of the normal phenotype of ganglion cells. For example, Perry et al. (1984) concluded that "…the conspicuous beading of Pα and Pβ dendrites… is not a histological artefact". Similarly, Wang et al. (2003) found "numerous bulb-shaped varicosities… in unmyelinated intraretinal ganglion cell axons… in all human specimens studied" and concluded that "… it is not likely that they represent pathologic and/or age-related changes."

However, these contrast with the smooth, bead-free processes of ganglion cell dendrites and axons imaged *in vivo* (e.g., Gray et al., 2008) and of ganglion cells maintained in organotypic culture (Greenberg et al., 2011). Is bead formation an artifact of tissue processing and, if so, can it be prevented? Based in part on studies of other neuronal preparations, we test here the possibility that bead formation is induced by FA concentration, fixative osmolarity, temperature, and Na^+ influx via voltage-gated Na^+ channels or glutamate-gated cation channels (Greenwood and Connolly, 2007). Our results indicate that retinal ganglion cells differ from hippocampal, cerebellar, cortical, and spinal

cord neurons in that beading is not precluded by glutamate receptor antagonists, tetrodotoxin, extracellular Ca^{2+} ion exclusion, or temperature shifts (cf., Bindokas and Miller, 1995; Emory and Lucas, 1995; Park et al., 1996; Hasbani et al.,1998; Al-Noori and Swann, 2000; Oliva et al., 2002; Kirov et al., 2004; Takeuchi et al., 2005; Zhang et al., 2007). Moreover, we describe a modification of FA-based fixatives that prevents bead formation in adult rat and rabbit retinal ganglion cells.

MATERIALS AND METHODS

Animals

Long-Evans rats (female; P60-P120; 150–250g; RRID:RGD_60991) were obtained from a commercial supplier (Harlan Bioproducts; San Diego, CA) and housed in standard cages at ~23°C on a 12-hr/12-hr light/dark cycle. Prior to enucleation, rats were killed by a lethal dose of sodium pentobarbital (150 mg/kg, i.p.; see below for the source of all chemicals used in this study). All animal care and experimental protocols were approved by the Animal Use and Care Administrative Advisory Committee of the University of California, Davis.

New Zealand white rabbits (2.5 kg) were obtained from a commercial supplier (Western Oregon Rabbit Co.; Philomath, OR), housed in standard cages at ~23 °C on a 12-hr/12-hr light/dark cycle, anesthetized, and killed in accordance with protocols approved by the Office of Laboratory Animal Care at the University of California, Berkeley. The eyes were quickly enucleated and the retinae isolated under dim red light.

The results from rat and rabbit retinae are pooled below because we observed qualitatively indistinguishable morphological changes in the sucrose-free fixatives we tested, and because sucrose supplementation blocked bead formation in both species.

Biolistic gene transfer and organotypic culture

DNA constructs were generated using standard molecular biology protocols. All constructs were fully sequenced to check for accuracy of the cloning procedure. The plasmid pCAG-eGFP-WPRE contains a hybrid cytomegalovirus enhancer and chickenbeta actin promoter (CAG) driving expression of enhanced green fluorescent protein (eGFP), followed by the woodchuck hepatitis virus posttranslational regulatory element (WPRE). Plasmid sequences are available upon request. Plasmid DNA (25 μg) was precipitated onto 1.6-μm gold microparticles and delivered *ex vivo* to freshly dissected rat and rabbit retina whole-mount cultures as described by Koizumi et al. (2007). To achieve sparse GFP labeling, microparticles were propelled through two 20-μm nylon mesh screens (Small Parts, Inc.; Miami Lakes, FL) that were placed 1 cm above the retina. Immediately after gene transfer, whole-mount retina cultures were incubated in darkness, in a light-tight incubator, at 35 °C and 5% CO_2 for 18–20 hr in Ames' culture medium supplemented with 1% horse serum, 1% N-2, 100 U/mL penicillin, 100 U/mL streptomycin, and 0.3 mg/mL L-glutamine. The pH of this solution was adjusted to 7.2–7.3 with NaOH. The osmolality was adjusted to 290–310 mmol/kg with sucrose. Each retina was supported on a cell culture insert (PICM0RG50, 0.4 μm Millicell, Millipore; Tuliagreen, Ireland) in the center of a 35-mm tissue culture dish.

Time-lapse imaging

Gene-gun transfected retinae were transferred from the incubator to the stage of a stereo microscope (SteREO Discovery.V8, Zeiss; Thornwood, NY), and viewed through a 1.5X objective (Achromat S, Zeiss) and a GFP+/eGFP filter cube (KSC 295-833D, Zeiss). GFP-expressing cells were identified as RGCs on the basis of an axon projecting into the nerve fiber layer and dendrites arborizing in the inner plexiform layer. Images were collected with a high resolution CCD camera (ORCA-ER, Hamamatsu Photonics K.K.; Hamamatsu, Japan) and an imaging software package (HCImage, Hamamatsu). The retinae were superfused at room temperature with the solutions and fixatives described in the Results section.

Fixation

Gene-gun transfected retinae were left adhered to filter supports, immersed in fixative solution, and slowly agitated on a rotator at room temperature. Table 1 lists the composition of the fixative buffers used in this study, with the osmolalities of each buffer measured with a vapor pressure osmometer (5520, Wescor; Logan, UT). The standard fixative solution (referred to hereafter as “standard FA”) contained 4% w/v formaldehyde (FA) in phosphate-buffered saline (PBS; consisting of 2.97 mM dibasic sodium phosphate, 1.06 mM monobasic potassium phosphate, 155 mM sodium chloride; Ca^{2+}-free, 10X dilution of 70011-044, Life Technologies; Grand Island, NY). In some experiments, this fixative was modified by varying the FA concentration, reducing the Na^+ concentration, adding tetrodotoxin (TTX), and/or adding glutamate receptor antagonists. The concentration of FA was varied between 4% and 0.8% (w/v in PBS) to control for the effects of fixative osmolarity (Margo and Lee, 1995). The PBS was replaced with Sørensen’s phosphate buffer (PB; consisting of 33.5 mM dibasic sodium phosphate and 33.5 mM monobasic sodium phosphate) to form a low-Na^+ (LS) fixative. Fixatives were supplemented with TTX (1 μM) to block persistent and transient voltage-gated Na^+ currents (Hidaka and Ishida, 1998; Margolis and Detwiler, 2007) and/or with a combination of (RS)-3-(2-carboxypiperazin-4-yl)-propyl-1-phosphonic acid (RS-CPP, 10 μM), 6-cyano-7-nitroquinoxaline-2,3-dione (CNQX, 10 μM) and L-(+)-2-amino-4-phosphonobutyric acid (L-AP4, 20 μM) to preclude glutamate responses (Slaughter and Miller, 1981; Kay and Ikeda, 1989; Mittman et al., 1990). Tissue was immersed in these fixatives for 30–120 min.

In an alternative protocol, tissue was immersed in an ice cold pre-fixative conditioning solution containing sucrose (200 mM) in PB for 30 min. Tissue was then immersed overnight in an ice-cold fixative solution, referred to as the protectant fixative, containing FA diluted to 4% in PB and supplemented with sucrose (200 mM). In some experiments, the conditioner and protectant fixative solutions were supplemented with a combination of TTX and the glutamate antagonists listed above.

For immunostaining, whole retinae were freshly dissected in ice cold PBS and flat mounted to black Isopore membrane filters (HTBP01300, Millipore). These retinae were then immersed overnight in ice cold fixative solutions of 4% FA diluted in either PBS, PB, or HEPES (134 mM). These fixatives were tested with and without supplementation with 200 mM sucrose.

Immunohistochemistry

Retinae were immunohistochemically processed as flat mounts. Fixed retinae were rinsed in Tris-buffered saline (TBS; 100 mM, pH 7.0), quenched for 30 min in glycine (1% w/v), and blocked and permeabilized overnight at 4 °C in PBS (pH 7.4) supplemented with bovine serum albumin (BSA, 0.5% w/v), Triton X-100 (0.05% w/v), and normal donkey serum (5% v/v). Retinae were incubated in primary antibodies overnight at 4 °C, rinsed in PBS, and incubated in secondary antibodies overnight at 4°C. Primary antibodies were diluted in PBS supplemented with BSA (0.5% w/v) and Triton-X 100 (0.1% v/v).

Antibody characterization

Table 2 lists the primary antibodies used in this study. Each is listed in the Journal of Comparative Neurology Antibody Database V.14 (http://onlinelibrary.wiley.com/journal/10.1002/(ISSN)1096-9861/homepage/jcn_antibody_database.htm,RRID:NLX_143660).

Signal attributed to GFP was amplified with an Alexa Fluor 488-conjugated rabbit polyclonal antibody against green fluorescent protein (GFP), raised against GFP isolated from *Aequorea victoria* and diluted to 2 μg/mL (Life Technologies, Cat# A-21311, RRID:AB_10058149). This antibody has been used in rodent retina previously (Xu and Tian, 2006; Stradleigh et al., 2011), and we detected no binding of this antibody in rat or rabbit retinae unless GFP expression was induced.

The rabbit polyclonal anti-melanopsin antibody (Thermo Fisher Scientific, Cat# PA1-781, RRID:AB_2156044) was generated against amino acids 1–19 of rat melanopsin and diluted to 0.3 μg/mL. The binding of the antibody has been characterized immunohistochemically in rat (Ingham et al., 2009) and mouse (Perez et al., 201) retinae, and by Western blot (Hattar et al., 2002). Signal attributed to melanopsin was visualized with an Alexa Fluor 555-conjugated, donkey-derived anti-rabbit polyclonal antibody (Life Technologies, Cat# A31572, RRID:AB_10562716).

The mouse monoclonal anti-200 kD neurofilament (NFH) antibody (Abcam, Cat# AB73273, clone SMI-32, RRID:AB_1566483) was generated against homogenized rat hippocampus and diluted to 0.3 μg/mL. This antibody has been characterized by immunohistochemistry in rat retina (Rodriguez et al., 2014) and immunoblots of mammalian brainstem and spinal cord (Sternberger and Sternberger, 1983; Goldstein et al., 1987). Signal attributed to NFH was visualized with an Alexa Fluor 488-conjugated, donkey-derived anti-mouse polyclonal antibody (Life Technologies, Cat# A21202, RRID:AB_10049285).

Confocal imaging

Confocal images were acquired on a laser scanning confocal microscope. Excitation was provided by Ar (488 nm), green He-Ne (543 nm), and red He-Ne (633 nm) lasers. Images were collected on two separate confocal systems. Some images were collected on a FluoView FV300 Confocal System (version 4.3, Olympus; Center Valley, PA) interfaced to an Olympus IX-70 inverted microscope. Data were collected using an oil immersion 40X objective in series of optical sections at intervals of 0.35–1 μm, with two- or three-frame Kalman averaging for each section. Other images were collected on a FluoView FV1000

Confocal System (version 1.6, Olympus) interfaced to an Olympus IX-81 inverted microscope. Data were collected with an oil immersion 60X objective in series of optical sections at 0.44-μm intervals, with three-frame Kalman averaging for each section.

Data analysis

Confocal data sets were imported into ImageJ, V1.47 (http://rsb.info.nih.gov/ij/,RRID:NIF-0000-30467). Adjacent optical sections were sometimes merged to form a projected image. Somatic diameter was determined by tracing a polygon around the perimeter of the cell body, measuring the polygon area, and calculating a diameter by assuming a circular profile. Beads were defined as bilateral, symmetrical swellings (cf., Price and Powell, 1970) greater than 30% of average neurite diameter. Bead diameter was measured by drawing a straight line through the widest region of the bead perpendicular to the neurite's long axis. Swellings larger than 3 standard deviations above the mean bead diameter were attributed to other neurite artifacts (Charras, 2008) and excluded from analysis. A segmented line was traced over each neurite and used to determine the distance from the soma to each bead, the distance between adjacent beads (i.e., interbead distance), and bead frequency (i.e., inverse of interbead distance). Statistical analysis of bead diameters, interbead distances, and bead frequency was performed using Excel 2013 (Microsoft; Redmond, WA).

Reagents

Reagents were obtained from the following sources: Abbott (Chicago, IL): sodium pentobarbital (0074-378-05); Affymetrix (Santa Clara, CA): HEPES, pH 7.3 (16924); Calbiochem (San Diego, CA): tetrodotoxin (584411); Jackson ImmunoResearch (West Grove, PA): normal donkey serum (017000121); Life Technologies: L-glutamine (25030-081), N-2 Supplement (17502-048), penicillin/streptomycin (15140-122), phosphate-buffered saline (Ca^{2+}- and Mg^{2+}-free, pH 7.4; 70011-044); Tris (pH 8.0; AM9856); Sigma-Aldrich (St. Louis, MO): bovine serum albumin (A8806), horse serum (H1138), sodium phosphate dibasic (RES20908), sodium phosphate monobasic (71505); Thermo Fisher Scientific: Triton X-100 (BP151-100); Tocris Bioscience (Minneapolis, MN): CNQX [6-cyano-7-nitroquinoxaline-2,3-dione] (0190), L-AP4 [L-(+)-2-amino-4-phosphono butyric acid] (0103), (RS)-CPP [(RS)-3-(2-carboxypiperazin-4-yl)-propyl-1-phosphonic acid] (0173).

RESULTS

This study tests whether the shapes of retinal ganglion cell dendrites and axons are preserved by a commonly used formaldehyde-containing fixative, and whether preservation is improved by altering the formaldehyde concentration, removing NaCl, pharmacologically blocking voltage- and glutamate-gated Na^+ influx, or adding sucrose. Cells were imaged after inducing GFP expression, with initial comparisons made between retinae immersed in different fixatives, and further tests made by imaging cells before and during immersion in selected fixatives. Additional retinal fields were immunostained for epitopes associated with a limited number of cell types. The results are arranged below to illustrate the effects of formaldehyde alone, to test modifications that alleviate beading in other central neurons, and

to present evidence that different changes in a widely used fixative formulation block beading in retinal ganglion cells (referred to hereafter as RGCs).

Standard fixative

Following immersion for 30–120 min in standard FA (viz., formaldehyde diluted to 4% w/v in phosphate-buffered saline (PBS)), RGCs displayed beads along their axons, along all segments of their dendrites, and at dendritic branch points (Fig. 1).

The maximum breadth (i.e., "diameter") of dendritic beads ranged from 0.5 to 5.3 μm (mean = 2.0 μm; median = 1.7 μm; n = 296). The largest dendritic beads were found in the primary dendrites of cells with large polygonal somata and tapering dendrites (Fig. 1A), while the distal (i.e., peripheral) segments of dendrites displayed the smallest beads (Figs. 1A, D). Bead diameters generally decreased with distance from the soma (Figs. 1A, D), and the decline was steeper in tapering dendrites than in dendrites that were small in caliber along their entire length ($P << 0.01$; Fig. 1D).

The diameter of axonal beads ranged from 0.8 to 4.9 μm. The average diameter of axonal beads (mean = 2.2 μm; median = 2.3 μm; n = 66) did not significantly differ from that of dendrites (see above). However, axonal beads showed little change in bead diameter with distance to soma, and this trend differed from that found in beads of both tapering ($P < 0.01$) and non-tapering ($P = 0.04$) dendrites.

The length of the dendritic segment connecting adjacent beads ranged from 1.7 to 49.7 μm. The average interbead distance in axons (mean = 8.9 μm; median = 7.3 μm; n = 66) did not significantly differ from that in dendrites (mean = 7.9 μm; median = 6.3 μm; n = 296). However, the dendritic interbead distance decreased with distance from the soma, producing a notable increase in bead frequency in the peripheral portions of the dendritic fields ($P = 0.8$; Fig. 1E). By contrast, axonal bead frequency rose slightly within the first 100 μm from the soma, and then fell with further distance from the soma ($P = 0.03$; Fig. 1E).

Apart from the changes with distance noted above, we did not attempt to compare bead and neurite diameters from images collected only after fixation. Lacking pre-fixation dendrite and axon diameters, these images do not distinguish between the possibility that beads are (*i*) swellings separated by neurite segments of reduced diameter, (*ii*) swellings separated by neuritic segments of normal diameter, or (*iii*) normal-diameter foci flanked by neurite segments of reduced diameter. We address these possibilities below by use of time-lapse imaging, after comparing the ability of various fixative modifications to block bead formation. Until then, we will refer to the varicosities in dendrites and axons as beads, and to the formation of these varicosities as beading, without assuming that beads are swellings rather than points that maintain their pre-fixation diameter as adjacent lengths of neurites shrink.

Osmolarity

4% FA is hypertonic, measuring 1300 mOsm in unbuffered solution (Fox et al., 1985). To test whether beading is induced by elevation of the extracellular osmolarity by FA, we examined RGCs fixed in solutions containing 4%, 2%, and 0.8% FA diluted in PBS (cf.,

Margo and Lee, 1995). Beads were typically smaller in diameter at the lowest FA concentration, especially in larger caliber axons and primary dendrites near the somata from which they emerged (Fig. 2). However, at all FA concentrations, small-caliber dendrites and axons, and the thin distal dendritic segments of all cells, appeared to consist of disjointed punctae separated by strands of fluorescent signal.

An indistinct fluorescent haze was observed around the somata of many cells incubated in standard fixative solutions (arrows, Figs. 1–3). Time lapse images collected before and during exposure to FA (see below) showed that a fluorescent haze spread away from individual somata, rather than coalesced toward somata, consistent with the possibility that somata leaked GFP during the fixation process.

Low-Na^+ buffer, TTX, glutamate receptor antagonists, Na^+ and Ca^{2+} exclusion

Several different experimental conditions induce bead formation in the dendrites and axons of hippocampal, cerebellar, cortical, and spinal cord neurons (e.g., Ramón y Cajal, 1899; Bindokas and Miller, 1995; Emory and Lucas, 1995; Park et al., 1996; Kirov et al., 2004; Lavenex et al., 2009), and a number of treatments have been found to counteract this beading (Ramón y Cajal, 1899; Bindokas and Miller, 1995; Park et al., 1996; Hasbani et al., 1998; Al-Noori and Swann, 2000; Oliva et al., 2002; Kirov et al., 2004; Takeuchi et al., 2005; Zhang et al., 2007). For example, glutamate receptor agonists (e.g., kainate) and voltage-gated Na^+ channel agonists (e.g., veratridine) lead to marked beading, and this can be averted by exclusion of extracellular Na^+ and Ca^{2+} ions, addition of glutamate receptor antagonists, or inclusion of voltage-gated Na^+ channel antagonists (e.g., tetrodotoxin, lidocaine). Because rabbit and rat RGCs receive excitatory synaptic input from glutamatergic bipolar cells (Massey and Miller, 1988; Marc, 1999; Zhang and Diamond, 2009) and can spike repetitively during sustained depolarizations (Koizumi et al., 2007; Hayashida et al., 2009), we tested whether bead formation in RGCs is also averted by reducing voltage- and/or synaptically-gated Na^+ influx. For this purpose, we used either PBS (158 mM Na^+, 301 mmol/kg), low-Na^+ Sørensen's phosphate buffer (PB, 67 mM Na^+, 147 mmol/kg), or HEPES (134 mM, Na^+-free, 203 mmol/kg), along with added tetrodotoxin (TTX, 1 μM) and/or a mixture of glutamate receptor antagonists [CPP (10 μM), CNQX (10 μM), and L-AP4 (20 μM)]. Ca^{2+} was not included in any of these buffers (Table 1).

Beads were seen throughout the dendrites and axons of RGCs immersed for up to 24 hrs in 4% FA diluted in either PB with TTX (i.e., "low-Na^+ solution"), PB augmented with glutamate receptor antagonists, PB with added TTX and glutamate receptor antagonists (i.e., "low-Na^+ and antagonist", or LSA, solution), or HEPES (Figs. 3, 5). Images collected at high magnification showed substantial beading in proximal and distal dendrites, beading (and barely perceptible interbead segments) in axons, and the perisomatic haze noted above (arrow, Fig. 3A).

Protectant fixative

Sucrose inclusion has been reported to reduce beading (Hasbani et al., 1998; Kirov et al., 2004; Greenwood et al., 2007) and guard extracellular space against shrinkage (Cragg, 1980). In part because we know of no published light microscopic images of retinae fixed in

sucrose, we tested whether sucrose blocks the formation of beads in RGCs. For an initial comparison with the beaded axons and dendrites of RGCs immersed in LSA fixative (PB, glutamate receptor antagonists, and TTX; Figs. 3A,B), we imaged GFP-expressing RGCs following immersion in LSA fixative that was supplemented with 200 mM sucrose. These RGCs displayed dendritic trees and axons with little or no beading. Confocal images collected at high magnification show that the dendrites tapered smoothly from their most proximal segments (where they emerge from each cell body) to their distal tips (Fig. 3C) and that even small-caliber axons were smoothly contoured, continuous, and bead-free (Fig. 3D). RGCs imaged at low magnification demonstrate bead-free processes throughout their dendritic trees and in the segments of axons further from the cell body (Fig. 3D).

To further test whether fixation in the presence of sucrose yielded bead-free RGCs, we imaged RGCs fixed after removing the glutamate receptor antagonists and TTX from the fixative used in Figures 3C, D. The fixative in these experiments thus contained 67 mM Na^+, no added Ca^{2+}, and 200 mM sucrose. Images collected at high-and low-magnifications show a similar absence of beads in proximal dendrites and proximal axon segments (Fig. 3E), as well as distal dendrites and distal axon segments (Fig. 3F) of RGCs. Together, Figures 3C–F show that sparsely, moderately, and densely branched dendritic arbors were bead-free in sucrose-supplemented fixative, unlike the bead-filled, similarly branched dendrites we observed in sucrose-free fixatives (Figs. 1, 2, 5, 6). Because bead-free RGCs were more numerous in sucrose-supplemented fixatives than in sucrose-free fixatives, we will refer to sucrose-supplemented fixatives as “protectant” fixatives. Unlike the RGCs fixed in standard FA, we observed no sign of GFP leakage from RGC somata in protectant solutions, regardless of whether they were supplemented with TTX and glutamate receptor antagonists.

Notably, although the osmolality of the protectant buffer is slightly greater than that of PBS (Table 1), the osmolarity of 4% formaldehyde in water (Fox et al., 1985) is four-fold greater. Assuming that the osmolality of each buffer is low enough that it is equivalent to its osmolarity, the osmolarity of the protectant fixative differs little (~3%) from that of standard FA.

Confocal imaging of retinae immunostained for neurofilament H and melanopsin

To test whether these fixation methods are applicable to neuronal compartments visualized by immunohistochemistry, freshly dissected retinae were flat mounted, immersion-fixed in standard, low-Na^+, or sucrose-supplemented FA solutions, and immunostained with antibodies raised against neurofilament H (NFH) or melanopsin. The binding of each primary antibody was visualized using a fluorophore-conjugated secondary antibody and a laser scanning confocal microscope.

NFH-like immunoreactivity was found in large somata in the ganglion cell layer (GCL), dendrites extending into the inner plexiform layer (IPL), and individual large-caliber axons and axon bundles in the nerve fiber layer (NFL), as in previous studies (Rodriguez et al., 2014). As in fields containing GFP-expressing RGCs with similarly large somata and tapering dendrites (Figs. 1A, 2A, 6, 7), the dendrites and axon-like processes were

extensively beaded in standard FA (Fig. 4A). By contrast, both dendritic and axonal beads were absent in FA supplemented with 200 mM sucrose (diluted in PB; Fig. 4B).

The dendrites of melanopsin-immunopositive RGCs differed distinctly from these in that their entire lengths (including the primary segments) were heavily beaded following immersion in either standard or protectant fixatives (Figs. 4C, D), and in that similar bead diameters and interbead distances were found in all three fixatives. These resemble varicosities reported in previous studies of intrinsically photosensitive RGCs (Hattar et al., 2002; Schmidt and Kofuji, 2009).

Unlike the anti-melanopsin antibody, the anti-NFH antibody labeled RGCs with large somata and tapering dendrites. Because the dendrites and axons of similar cells were extensively beaded in standard FA (Fig. 1), and this beading was not precluded by TTX and glutamate receptor antagonists (Fig. 3), we compared NFH-immunopositive neurites following fixation in FA that was diluted in either PBS or HEPES. The immunopositive axon-like neurites were beaded to similar extents following fixation in PBS (Fig. 5A) and HEPES, and similar beading was observed in hypotonic (Fig. 5C) and hypertonic (Fig. 5E) HEPES. Consistent with our observation that sucrose blocked beading in hypotonic PB (Figs. 3E, F), 200 mM sucrose blocked beading if the FA was diluted in hypotonic HEPES (Fig. 5D). By contrast, 200 mM sucrose failed to block beading if the FA was diluted in PBS (Fig. 5B) or in hypertonic HEPES (Fig. 5F). This implies that sucrose can block beading if it contributes a significant portion of the total buffer osmolarity (see Discussion).

Time lapse imaging of retinal ganglion cells during fixation

To test whether protectant solutions preserve the structure of live cells, we organotypically cultured GFP-expressing RGCs (Koizumi et al., 2007; Greenberg et al., 2011) and collected time-lapse images both before and after superfusion with fixative solutions.

Standard fixative—The dendrites and axons of the unfixed GFP-expressing RGCs we observed were generally devoid of varicosities. This facilitated testing whether protectant solutions preserve the structure of live cells and, at the same time, limited our ability to test whether varicosities are normal features of some types of RGC. Fig. 6 illustrates smoothly contoured dendrites and axons in one cell possessing a densely branched, ovoid dendritic field (Fig. $6A_1$) and another cell with an elliptical dendritic field (Fig. $6B_1$). The sequences of images collected from these cells show that immersion in standard FA induces bead formation in dendrites and axons. In all of the cells we imaged both before and after immersion in standard FA (n = 11) in a total of 8 retinae, beads formed in the axons and dendritic fields after exposure to the fixative. To minimize GFP bleaching, we collected images at 15- to 30-sec intervals. Although this prevented us from resolving the time course of bead formation in detail, we found that beading began within 30 sec of immersion in standard FA in some cells (Fig. $6B_2$). Additional beads formed in the axon and in the remainder of the dendritic field over several subsequent minutes (5 min; Fig. $6B_3$). Other RGCs were more resistant to beading, taking as long as 6 min to start beading (at the distal dendritic segments in Fig. $6A_2$), exhibiting beads throughout the dendritic field and axon within 7.5 min, and exhibiting maximal beading within a total of 10 min exposure to the

standard FA (Fig. 6A_3). Given that fixatives may have contacted and bathed RGCs at different rates in our preparations for various reasons (e.g., overlying vitreous, retinal vasculature, glial cells, and, in the case of displaced RGCs, neuronal processes), we did not attempt to measure, or account for, differences in the onset or rate of bead formation. Notwithstanding this, our primary observation in this data set is that exposure to standard FA can induce bead formation in RGC dendrites and axons when compared to their unfixed state. As in cortical and hippocampal neurons (Park et al., 1996; Hasbani et al., 1998; Oliva et al., 2002), these beads formed within minutes.

Standard FA also appeared to induce GFP efflux from the somata of at least some RGCs, as evidenced by the fluorescent haze around the cell body after prolonged exposure (Figs. 1–3). This is reminiscent of post-fixation leak of some intracellularly injected fluorescent dyes (e.g., Stewart, 1978), and time-lapse images show that the GFP haze appeared after beads form. We assume that this efflux is passive leakage.

Protectant fixative—GFP-expressing RGCs showed little (if any) change in neurite contour and diameter between the periods before fixation and after immersion in protectant fixative. The unfixed RGC in Fig. 7A_1 possesses a sparse, radial dendritic field and an axon devoid of visible varicosities. Even after 10 min of immersion in protectant fixative, these cellular processes appeared unchanged (Fig. 7A_2). Because we found little or no beading in tissue exposed to protectant fixative, both at room temperature and on ice, our results indicate that beading is not induced by chilling as reported for hippocampal and spinal cord neurons (Emory and Lucas, 1995; Kirov et al., 2004; Zhang et al., 2007).

To test whether the formation of beads is a time-dependent process initiated by the removal of the tissue from culture conditions and occurs regardless of buffer composition, we immersed GFP-expressing RGCs in various buffer solutions in series. The unfixed RGCs visible in Fig. 7B_1 show overlapping dendritic trees, both of which possess smooth, gradually tapering dendrites and a continuous axon. Immersion in a conditioning solution (i.e., protectant solution without FA) for 11 min produced no gross change in the morphology of either cell (Fig. 7B_2). Removal of conditioning solution and the addition of protectant fixative also did not noticeably alter RGC structure, even after 5 min in protectant fixative (i.e., after 16 min elapsed after removal from culture conditions and immersion in solutions; Fig. 7B_3). It is only after the removal of protectant fixative and the addition of standard FA that the cells begin to form beads in their processes. Beads formed throughout the dendritic arbors and axons of both RGCs within 5 min of incubation in standard FA (Fig. 7B_4), as readily as in retinae immersed directly into standard FA (n = 6; e.g., Fig. 6).

Beads are swellings

The goal of the above experiments was to find conditions that prevent fixative-induced beading in RGCs, rather than to resolve whether beads are swellings *per se*. In superimpositions of time-lapse images collected from RGCs before and after exposure to standard FA, post-fix beads in axons (Fig. 8A_3) and in dendrites (Figs. 8A_3, 8B_3) are larger in diameter than the corresponding points prior to fixation. In the same images, some of the interbead segments in dendrites (Figs. 8A, 8B) are smaller in diameter after fixation than the

corresponding segments prior to fixation. Some, but not all, interbead segments of the axons show similar shrinkage. Given the limited spatial resolution of our images, and the small diameter of most portions of the dendrites and axons, we did not attempt to quantify increases or decreases in the size of these structures. We also did not test the possibility that the fluorescence intensity faded in the interbead segments (cf., He et al., 1999). However, our images show no conspicuous shortening of the distance from the somata to the dendrite arbor branch points (Fig. 8). This implies that the interbead segments and the total length of the dendrites did not appreciably shorten in order to allow beads to increase in diameter.

DISCUSSION

The results of this study show that a widely used formaldehyde-based (FA) fixative can induce the formation of varicosities in adult mammalian retinal ganglion cell (RGC) dendrites and axons. Although previous studies have found beaded dendrites and axons in FA-fixed retinae (e.g., Perry et al., 1984, Huxlin and Goodchild, 1997; Wang et al., 2003), our results show for the first time that RGC beading can be blocked. Below, we discuss properties of RGCs that might contribute to bead formation, and how our observations compare with studies of beading in other central neurons.

Bead formation in retinal neurons

FA can afford moderate structural preservation because it can penetrate tissue quickly and, upon spontaneous reduction and formation of methylene glycol, cross-link proteins via a condensation reaction and methylene bridge formation (Fraenkelconrat and Olcott, 1948; Fox et al., 1985; Metz et al., 2004; Sutherland et al., 2008). At the same time, some results suggest that FA may be a poor choice for terminating physiological responses and for stabilizing tissue. For example, FA prolongs voltage-gated Na^+ currents (Nonner et al., 1980; Gonoi and Hille, 1987), broadens spikes (Shrager et al., 1969), induces TTX-insensitive and Ca^{2+}-independent neurotransmitter release (Smith and Reese, 1980), and slowly depolarizes cells (Fozzard and Dominguez, 1969). Moreover, tissue typically remains osmotically active for as long as 24 hrs in FA (Paljärvi et al., 1979) and the fixation is largely reversed by washing (Helander, 1994; Sutherland et al., 2008; Shepherd et al., 2009). Our results provide clear evidence that FA does not rapidly stabilize retinal tissue, in that RGC dendrites and axons bead when exposed to standard FA (viz., FA diluted in sucrose-free PBS), even after incubation for more than 10 min in a protectant, sucrose-containing FA solution that blocks beading (Fig. $6B_4$). This is consistent with the slow fixation of other tissues by FA (Fox et al., 1985), especially at neutral pH (Berod et al., 1981), and the limited ability of FA to cross-link reactive groups, especially by comparison with glutaraldehyde (Peters and Ashley, 1967).

Because we found no noticeable bead formation in protectant fixatives, our results show that the inclusion of FA does not necessarily cause beading. It would be natural to ask if beading occurs under other conditions intended to maintain cell shape and to ask what causes beading. In fact, beading can be seen in RGC dendrites and axons, and also amacrine cell dendrites, in preparations fixed in either dichromate or picric acid (Golgi, 1873; Plate VII of Tartuferi, 1887; Plates XX and XXI of Dogiel, 1891). Moreover, beads can form in the

dendrites and axons of RGCs imaged *ex vivo* in the absence of FA, despite their absence when the same cells were imaged *in vivo* (Gray et al., 2008). While we know of no direct measurements of RGC viability under these conditions, retinae stop responding to light within 2–6 min of exposure to FA (Hamasaki, 1964) and our results show that FA does not fix retinae within less than 10 min. Although it remains to be tested how beads form, this is reminiscent of Ramón y Cajal's statements regarding bead formation in hippocampal pyramidal neurons:

> "We believe that these varicosities result from postmortem changes that take place in all neurons within half an hour to an hour after death… most convincingly, one can see these beads or varicosities form before one's very eyes."

(Ramón y Cajal, 1899). Thus, our results suggest that preservation of cellular morphology by FA (and, for that matter, other fixatives) would entail either rapid stabilization (i.e., within a few minutes or less) or measures that preclude distortion (e.g., replacement of Na^+ by sucrose). Although we have not examined RGCs in other species, the varicosities in *ex vivo* RGCs of multiple species and classes (e.g., frog: Kock et al., 1989; quail: Muchnick and Hibbard 1980; cat: FitzGibbon et al., 1991; ferret: Wingate et al., 1992; marmoset: Walsh et al., 1999; macaque: Watanabe and Rodieck, 1989) suggest that our results are not limited to rat and rabbit.

Bead formation in other central neurons

Because beading in other central neurons does not occur in FA if the external Na^+-containing medium is supplemented with sucrose, previous investigators have suggested that FA induces Na^+ influx, and that this leads to elevated cytoplasmic osmolarity, water influx, and bead formation (e.g., Hasbani et al., 1998; Greenwood et al., 2007). Our results address this possibility in three ways.

Firstly, RGC beading clearly differs from that in hippocampal, cerebellar, cortical, and spinal cord neurons in that it is not blocked by tetrodotoxin (Hasbani et al., 1998; Ikegaya et al., 2001), glutamate receptor antagonists (Park et al., 1996; Al-Noori and Swann, 2000; Oliva et al., 2002; Takeuchi et al., 2005), or Ca^{2+} omission (Bindokas and Miller, 1995), and it is not induced by low temperature (Emory and Lucas, 1995; Kirov et al., 2004; Zhang et al., 2007). This conclusion is most directly supported by our observation that beading occurs in Na^+- and Ca^{2+}-free fixative (viz., FA diluted in HEPES; Fig. 5B), and that beading does not occur if the Na^+/Ca^{2+}-free fixative is supplemented with sucrose (Fig. 5D). By itself, inclusion of TTX to block voltage-gated Na^+ currents and antagonists that block glutamate receptor-mediated light responses would not have excluded the possibility of Na^+ influx, because TTX-resistant Na^+ channels have been found in RGCs (Mirshani et al., 1999; Brockway et al., 2002).

Secondly, superimposition of images collected from single RGCs before and after exposure to standard FA show that dendritic and axonal beads are larger in diameter than the same point prior to fixation, and that at least some interbead segments of neurites are smaller in diameter than the same segments prior to fixation (Fig. 8). While it seems unlikely that water influx can produce both bead swelling and interbead segment shrinkage, interbead

segments might shrink due to water efflux upon initial exposure to the hypertonic fixative (Cragg, 1980). How beads expand in membrane surface area (e.g., by wresting membrane from adjacent segments of the neurite) remains to be established (see Diz-Muñoz et al., 2013). As in other beaded preparations, glutamate receptor activation, Na^+ influx, and increases in intracellular Ca^{2+} concentration can occur in RGCs; mitochondria, smooth endoplasmic reticulum, and small numbers of microtubules have been found inside RGC axonal beads (Greenberg et al., 1990; Wang et al., 2003); the interbead segments of RGC axons are filled predominantly by cytoskeletal elements (Greenberg et al., 1990; Wang et al., 2003); and the bead diameters in our confocal images (Fig. 1) are larger than the girth of mitochondria in control RGCs (< 1 μm; Carelli et al., 2004; Davis et al., 2014). On the other hand, it is not yet known whether other events that cause or precede beading in other cells also occur in RGC dendrites and axons (e.g., ATP depletion, water influx, microtubule depolymerization, and enlargement of individual mitochondria as opposed to fusion of multiple mitochondria).

Thirdly, our results show that beading occurs in buffers that differ in osmolality and Na^+ content (Table 1), including isotonic (PBS), hypotonic (LS, LSA, 134 mM HEPES), and hypertonic (300 mM HEPES) buffers; and normal-Na^+ (PBS), reduced-Na^+ (LS, LSA), and Na^+-free (HEPES) buffers. Moreover, our results show that beading is prevented in sucrose-supplemented buffers that are either nearly isotonic (protectant solution) or moderately hypertonic (134 mM HEPES + sucrose). These results indicate that bead formation can be blocked by replacing extracellular Na^+ with sucrose. This is consonant with the finding of other studies that isotonic sucrose improves brain tissue preservation (Cragg, 1979), blocks cold-induced beading in hippocampal neurons (Kirov et al., 2004), and preserves cell viability and synaptic function during brain slice preparation (Aghajanian and Rasmussen, 1989; Isope and Barbour, 2002). Although we know of no similar comparison of RGC morphology in other sucrose-free and sucrose-supplemented fixatives, previous studies have found that optic nerve axons were varicose after fixation in sucrose-free glutaraldehyde (Freeman, 1978), that RGC dendrites and axons were varicose after fixation in a sucrose-free mixture of glutaraldehyde and paraformaldehyde (Stanford, 1987), and that intraretinal segments of RGC axons were bead-free after fixation in a sucrose-supplemented mixture of glutaraldehyde and paraformaldehyde (Marc, 1999; Marc and Jones, 2002). These results are of interest because they indicate that beads can form despite use of a fixative that blocks spikes, transmitter release, and voltage-gated ion currents (Shrager et al., 1969; Rosenmund and Stevens, 1997), and that binds amino acids to proteins more efficaciously and stably than FA (Peters and Ashley, 1967). Moreover, these results indicate that preservation of cell morphology can be improved by including sucrose in fixatives used for light microscopic immunohistochemistry, staining, and imaging, and not only for transmission electron microscopy (Sabatini et al., 1963).

This comes with two caveats. First, we did not test whether beading is impeded or blocked by impermeant substances other than sucrose. Second, while our results do not exclude the possibility that sucrose prevents beading by increasing the osmolarity of the hypotonic buffers we used (e.g., 134 mM HEPES), sucrose may help preserve neurite contour in other ways. While 200 mM sucrose blocked beading when added to hypotonic buffers (Figs. 4B, 5D), beading was not blocked by adding the same amount of sucrose to normal PBS (Fig.

5B) or to 300 mM HEPES (Fig. 5F), or by raising the HEPES concentration from 134 mM to 300 mM in the absence of sucrose (Fig. 5E). Consistent with reports that swelling and ultrastructural damage of renal tubule cells are blocked if approximately 50% of the total buffer osmolarity is due to sucrose (Coffey and Andrews, 1983), RGC beading in PBS or 300 mM HEPES is prevented if the sucrose concentration is doubled to 400 mM (results not illustrated). We did not use these formulations routinely because the RGC axons appeared to be compressed axially into accordion-like ripples after immersion of some preparations in these highly hypertonic solutions, perhaps due to linear shrinkage (results not illustrated).

Applicability

Some previous studies found varicosities in certain types of RGCs and not others (Kolb et al., 1992; Lin et al., 2000; Rockhill et al., 2002; Coombs et al., 2006). Although we focused the present study on RGCs that displayed little or no dendritic or axonal beading in culture media and protectant fixatives, one exception is that we found beading throughout the dendrites of melanopsin-immunopositive RGCs following immersion in either standard or protectant fixatives (Fig. 4). This indicates that phenotypically normal varicosities were not necessarily lost under the conditions of our experiments.

Varicosities in some retinal amacrine cells are sites of neurotransmitter release (Pourcho, 1982; Famiglietti 1983; Voigt and Wässle, 1987). Consistent with these results, we found varicosities in the dendrites of tyrosine hydroxylase-immunopositive amacrine cells in either standard or protectant fixatives (unpublished observations). Although fish RGC dendrites have been found to synapse onto other neurons (Sakai et al., 1986), the synapses were found at far lower densities than the beading we have observed and we know of no report that mammalian RGC dendrites form morphological synapses.

In summary, we have identified conditions that block the artifactual formation of beads in FA-fixed RGC dendrites and axons. This should facilitate purely morphological studies, e.g., distinguishing axon diameters in transverse sections (rat: Forrester and Peters, 1967; rabbit: Vaney and Hughes, 1976), cluster analyses of cell types (De Juan et al., 1992; Badea and Nathans, 2004), and assessing impacts of diseases on ganglion cell morphology (Gastinger et al., 2008; Margolis et al., 2008; Mazzoni et al., 2008). Beaded axons differ in diameter when sectioned at swellings versus interbead segments and, to the extent that they include the diameter of swellings and interbead segments, single transverse sections through axon bundles (intraretinal, optic nerve, optic tract) are unlikely to account for the conduction velocities of unfixed axons. It will be of interest to measure axon diameters from preparations immersed in sucrose-supplemented fixatives and compare these with spike conduction velocity (cf., Bishop et al., 1953; Stone and Holländer, 1971; Boycott and Wässle, 1974; Freeman, 1978). Likewise, the space constant of beaded and smoothly contoured neurites are expected to differ (e.g., Ellias and Stevens, 1980). Labeling entire individual cells within populations of specific cell types (see references cited in the Introduction) should facilitate systematic measurements of the diameter and taper of smooth dendrites, and the size and distribution of phenotypically normal beads, across entire retinae.

Sucrose-supplemented fixatives should also facilitate the use of FA to cross-link reactive molecules while preserving cell shape, e.g., for immunohistochemical localization of

integral membrane proteins, outer- and inner-leaflet proteins, signaling cascade components, and neurotransmitters (e.g., Barnstable and Dräger, 1984; Wollner and Catterall, 1986; Pow et al., 1995; Haverkamp and Wässle, 2000; Wayman et al., 2011). FA-based fixatives that do not induce beading have enabled us to visualize dendritic shape, contour, branching, and arborization (Stradleigh et al., 2011), contrast axon calibers (Stradleigh et al., 2011), gauge protein colocalizations (Stradleigh et al., 2011; Partida et al., 2012), and compare the binding of antibodies in dark- and light-adapted retinae (Ogata et al., 2012). Moreover, we have found that replacing NaCl by sucrose suppresses beading even if the fixative pH is shifted to alter fixation speed and efficacy (Berod et al., 1981; Eldred et al., 1983; Stradleigh et al., 2011; Ogata et al., 2012). The improved preservation of cells by the protectant fixatives we have described here is of particular interest because immunostaining with some antibodies (e.g., monoclonal and polyclonal antibodies directed against D1 dopamine receptors, HCN channel subunits, cAMP, and phosphorylated CaMKII) is compatible with FA-based fixatives (Pow et al., 1995; Hayashida et al., 2009; Stradleigh et al., 2011; Ogata et al., 2012) but not with a variety of other fixatives (e.g., Clarke's fluid, glyoxal, ice cold acetone; unpublished observations).

Acknowledgments

Some of these results were presented at the Fourth European Retina Meeting (October, 2013) in Alicante, Spain. The authors thank L. Peichl and W.K. Stell for translations and discussions, L. Peichl and D. Benzaid (Max Planck Institute for Brain Research) for scans of figures from Dogiel (1891), F.S. Werblin for support and use of facilities, and the anonymous reviewers for constructive comments.

Support: Grant sponsor: National Institutes of Health; Grant number: EY008120 (A.T.I.); P30 EY012576 (J.S. Werner); EY018790 (F.S. Werblin); Research to Prevent Blindness (to the Department of Ophthalmology, U.C. Davis); Grant sponsor: NIH-IMSD Fellowship (to T.W.S.), Grant number: R25 56765; Grant sponsor: NIH-NEI Training Grant Fellowship (to T.W.S.), Grant number: T32 EY015387; Grant sponsor: NIH Research Supplement to Promote Diversity in Health-Related Research (EY08120-17S1 to A.T.I.).

LITERATURE CITED

Aghajanian GK, Rasmussen K. Intracellular studies in the facial nucleus illustrating a simple new method for obtaining viable motoneurons in adult rat brain slices. Synapse. 1989; 3:331–338. [PubMed: 2740992]

Al-Noori S, Swann JW. A role for sodium and chloride in kainic acid-induced beading of inhibitory interneuron dendrites. Neuroscience. 2000; 101:337–348. [PubMed: 11074157]

Anderson JR, Jones BW, Yang JH, Shaw MV, Watt CB, Koshevoy P, Spaltenstein J, Jurrus E, U VK, Whitaker RT, Mastronarde D, Tasdizen T, Marc RE. A computational framework for ultrastructural mapping of neural circuitry. PLoS Biol. 2009; 7(3):e1000074. [PubMed: 19855814]

Anger EM, Unterhuber A, Hermann B, Sattmann H, Schubert C, Morgan JE, Cowey A, Ahnelt PK, Drexler W. Ultrahigh resolution optical coherence tomography of the monkey fovea. Identification of retinal sublayers by correlation with semithin histology sections. Exp Eye Res. 2004; 78:1117–1125. [PubMed: 15109918]

Arey LB. The occurrence and the significance of photomechanical changes in the vertebrate retina – an historical survey. J Comp Neurol. 1915; 25:535–554.

Badea TC, Nathans J. Quantitative analysis of neuronal morphologies in the mouse retina visualized by using a genetically directed reporter. J Comp Neurol. 2004; 480:331–351. [PubMed: 15558785]

Barnstable CJ, Dräger UC. Thy-1 antigen: a ganglion cell specific marker in rodent retina. Neurosci. 1984; 11:847–855.

Behrens UD, Kasten P, Wagner HJ. Adaptation-dependent plasticity of rod bipolar cell axon terminal morphology in the rat retina. Cell Tissue Res. 1998; 294:243–251. [PubMed: 9799440]

Berod A, Hartman BK, Pujol JF. Importance of fixation in immunohistochemistry: use of formaldehyde solutions at variable pH for the localization of tyrosine hydroxylase. J Histochem Cytochem. 1981; 29:844–850. [PubMed: 6167611]

Bhide PG, West WC, Fry KR, Frost DO. An immunocytochemical marker for hamster retinal ganglion cells. J Neurocytol. 1994; 23:167–177. [PubMed: 8006677]

Bindokas VP, Miller RJ. Excitotoxic degeneration is initiated at non-random sites in cultured rat cerebellar neurons. J Neurosci. 1995; 15:6999–7011. [PubMed: 7472456]

Bishop PO, Jeremy D, Lance JW. The optic nerve; properties of a central tract. J Physiol. 1953; 121:415–432. [PubMed: 13085344]

Boon ME, Kok LP. Theory and practice of combining coagulant fixation and microwave histoprocessing. Biotech Histochem. 2008; 83:261–277. [PubMed: 19031284]

Boycott BB, Wässle H. The morphological types of ganglion cells of the domestic cat's retina. J Physiol. 1974; 240:397–419. [PubMed: 4422168]

Brockway LM, Zhou ZH, Bubien JK, Jovov B, Benos DJ, Keyser KT. Rabbit retinal neurons and glia express a variety of ENaC/DEG subunits. Am J Physiol. 2002; 283:C126–134.

Bucher D, Scholz M, Stetter M, Obermayer K, Pflüger HJ. Correction methods for three-dimensional reconstructions from confocal images: I. Tissue shrinking and axial scaling. J Neurosci Methods. 2000; 100:135–143. [PubMed: 11040376]

Charras GT. A short history of blebbing. J Microscopy. 2008; 231:466–478.

Coffey AK, Andrews PM. Ultrastructure of kidney preservation: varying the amount of an effective osmotic agent in isotonic and hypertonic preservation solutions. Transplantation. 1983; 35:136–143. [PubMed: 6338633]

Cohen E, Sterling P. Demonstration of cell types among cone bipolar neurons of cat retina. Philos Trans R Soc Lond B Biol Sci. 1990; 330:305–321. [PubMed: 1982357]

Coombs J, van der List D, Wang GY, Chalupa LM. Morphological properties of mouse retinal ganglion cells. Neurosci. 2006; 140:123–136.

Cragg B. Brain extracellular space fixed for electron microscopy. Neurosci Lett. 1979; 15:301–306. [PubMed: 394033]

Cragg B. Preservation of extracellular space during fixation of the brain for electron microscopy. Tissue Cell. 1980; 12:63–72. [PubMed: 6987773]

Dacey DM, Peterson BB, Robinson FR, Gamlin PD. Fireworks in the primate retina: in vitro photodynamics reveals diverse LGN-projecting ganglion cell types. Neuron. 2003; 37:15–27. [PubMed: 12526769]

Davis CH, Kim KY, Bushong EA, Mills EA, Boassa D, Shih T, Kinebuchi M, Phan S, Zhou Y, Bihlmeyer NA, Nguyen JV, Jin Y, Ellisman MH, Marsh-Armstrong N. Transcellular degradation of axonal mitochondria. Proc Natl Acad Sci USA. 2014; 111:9633–9638. [PubMed: 24979790]

De Juan J, Cuenca N, Iñiguez C, Fernández E. Axon types classified by morphometric and multivariate analysis in the rat optic nerve. Brain Res. 1992; 585:431–434. [PubMed: 1511332]

Diz-Muñoz A, Fletcher DA, Weiner OD. Use the force: membrane tension as an organizer of cell shape and motility. Trends Cell Biol. 2013; 23:47–53. [PubMed: 23122885]

Dogiel AS. Ueber die nervoesen Elemente in der Retina des Menschen. Arch Mikrosk Anat. 1891; 38:317–344.

Eldred WD, Zucker C, Karten HJ, Yazulla S. Comparison of fixation and penetration enhancement techniques for use in ultrastructural immunocytochemistry. J Histochem Cytochem. 1983; 31:285–292. [PubMed: 6339606]

Ellias SA, Stevens JK. The dendritic varicosity: a mechanism for electrically isolating the dendrites of cat retinal amacrine cells? Brain Res. 1980; 196:365–372. [PubMed: 6249448]

Emery DG, Lucas JH. Ultrastructural damage and neuritic beading in cold-stressed spinal neurons with comparisons to NMDA and A23187 toxicity. Brain Res. 1995; 692:161–173. [PubMed: 8548300]

Famiglietti EV Jr. On and off pathways through amacrine cells in mammalian retina: the synaptic connections of "starburst" amacrine cells. Vision Res. 1983; 23:1265–1279. [PubMed: 6362185]

Fernandez E, Kolb H. A method for selective intracellular labeling of immunostained neurons in turtle retina. J Histochem Cytochem. 1993; 41:635–641. [PubMed: 7680680]

FitzGibbon T, Funke K, Eysel UT. Anatomical correlations between soma size, axon diameter, and intraretinal length for the alpha ganglion cells of the cat retina. Vis Neurosci. 1991; 6:159–174. [PubMed: 2049331]

Forrester J, Peters A. Nerve fibres in optic nerve of rat. Nature. 1967; 214:245–247. [PubMed: 4166494]

Fox CH, Johnson FB, Whiting J, Roller PP. Formaldehyde fixation. J Histochem Cytochem. 1985; 33:845–853. [PubMed: 3894502]

Fraenkelconrat H, Olcott HS. The reaction of formaldehyde with proteins. V. Cross-linking between amino and primary amide or guanidyl groups. J Am Chem Soc. 1948; 70:2673–2684. [PubMed: 18876976]

Freeman B. Myelin sheath thickness and conduction latency groups in the cat optic nerve. J Comp Neurol. 1978; 181:183–196. [PubMed: 681556]

Gardella D, Hatton WJ, Rind HB, Rosen GD, von Bartheld CS. Differential tissue shrinkage and compression in the z-axis: implications for optical dissector counting in vibratome-, plastic- and cryosections. J Neurosci Meth. 2003; 124:45–59.

Gastinger MJ, Kunselman AR, Conboy EE, Bronson SK, Barber AJ. Dendrite remodeling and other abnormalities in the retinal ganglion cells of $Ins2^{Akita}$ diabetic mice. Invest Ophthalmol Vis Sci. 2008; 49:2635–2642. [PubMed: 18515593]

Goldstein ME, Sternberger NH, Sternberger LA. Phosphorylation protects neurofilaments against proteolysis. J Neuroimmunol. 1987; 14:149–160. [PubMed: 3029175]

Golgi C. Sulla struttura della sostanza grigia del cervello. Gazz Med Lomb. 1873; 33:244–246.

Gonoi T, Hille B. Gating of Na channels. Inactivation modifiers discriminate among models. J Gen Physiol. 1987; 89:253–274. [PubMed: 2435840]

Grace AA, Llinás R. Morphological artifacts induced in intracellularly stained neurons by dehydration: circumvention using rapid dimethyl sulfoxide clearing. Neuroscience. 1985; 16:461–475. [PubMed: 2417160]

Gray DC, Wolfe R, Gee BP, Scoles D, Geng Y, Masella BD, Dubra A, Luque S, Williams DR, Merigan WH. In vivo imaging of the fine structure of rhodamine-labeled macaque retinal ganglion cells. Invest Ophthalmol Vis Sci. 2008; 49:467–473. [PubMed: 18172127]

Greenberg KP, Pham A, Werblin FS. Differential targeting of optical neuromodulators to ganglion cell soma and dendrites allows dynamic control of center-surround antagonism. Neuron. 2011; 69:713–720. [PubMed: 21338881]

Greenberg MM, Leitao C, Trogadis J, Stevens JK. Irregular geometries in normal unmyelinated axons: a 3D serial EM analysis. J Neurocytol. 1990; 19:978–988. [PubMed: 2292722]

Greenwood SM, Connolly CN. Dendritic and mitochondrial changes during glutamate excitotoxicity. Neuropharmacol. 2007; 53:891–898.

Greenwood SM, Mizielinska SM, Frenguelli BG, Harvey J, Connolly CN. Mitochondrial dysfunction and dendritic beading during neuronal toxicity. J Biol Chem. 2007; 282:26235–26244. [PubMed: 17616519]

Hamasaki DI. The electroretinogram after application of various substances to the isolated retina. J Physiol. 1964; 173:449–458. [PubMed: 14220263]

Hasbani MJ, Hyrc KL, Faddis BT, Romano C, Goldberg MP. Distinct roles for sodium, chloride, and calcium in excitotoxic dendritic injury and recovery. Exp Neurol. 1998; 154:241–258. [PubMed: 9875285]

Hattar S, Liao HW, Takao M, Berson DM, Yau KW. Melanopsin-containing retinal ganglion cells: architecture, projections, and intrinsic photosensitivity. Science. 2002; 295:1065–1070. [PubMed: 11834834]

Haverkamp S, Wässle H. Immunocytochemical analysis of the mouse retina. J Comp Neurol. 2000; 424:1–23. [PubMed: 10888735]

He S, Jin ZF, Masland RH. The nondiscriminating zone of directionally selective retinal ganglion cells: comparison with dendritic structure and implications for mechanism. J Neurosci. 1999; 19:8049–8056. [PubMed: 10479705]

Helander KG. Kinetic studies of formaldehyde binding in tissue. Biotechnic Histochem. 1994; 69:177–179.

Hidaka S, Ishida AT. Voltage-gated Na^+ current availability after step- and spike-shaped conditioning depolarizations of retinal ganglion cells. Pflügers Arch. 1998; 436:497–508. [PubMed: 9683721]

Hoffman EM, Schechter R, Miller KE. Fixative composition alters distributions of immunoreactivity for glutaminase and two markers of nociceptive neurons, Nav1.8 and TRPV1, in the rat dorsal root ganglion. J Histochem Cytochem. 2010; 58:329–344. [PubMed: 20026672]

Hoshi H, O'Brien J, Mills SL. A novel fluorescent tracer for visualizing coupled cells in neural circuits of living tissue. J Histochem Cytochem. 2006; 54:1169–1176. [PubMed: 16864895]

Huxlin KR, Goodchild AK. Retinal ganglion cells in the albino rat: revised morphological classification. J Comp Neurol. 1997; 385:309–323. [PubMed: 9268130]

Ingham ES, Gunhan E, Fuller PM, Fuller CA. Immunotoxin-induced ablation of melanopsin retinal ganglion cells in a non-murine mammalian model. J Comp Neurol. 2009; 516:125–140. [PubMed: 19575450]

Isope P, Barbour B. Properties of unitary granule cell–>Purkinje cell synapses in adult rat cerebellar slices. J Neurosci. 2002; 22:9668–9678. [PubMed: 12427822]

Kanjhan R, Vaney DI. Semi-loose seal Neurobiotin electroporation for combined structural and functional analysis of neurons. Pflügers Arch. 2008; 457:561–568. [PubMed: 18600343]

Kay CD, Ikeda H. The quinoxalinediones antagonise the visual firing of sustained retinal ganglion cells. Eur J Pharmacol. 1989; 164:381–384. [PubMed: 2569410]

Kim IJ, Zhang Y, Yamagata M, Meister M, Sanes JR. Molecular identification of a retinal cell type that responds to upward motion. Nature. 2008; 452:478–482. [PubMed: 18368118]

Kirov SA, Petrak LJ, Fiala JC, Harris KM. Dendritic spines disappear with chilling but proliferate excessively upon rewarming of mature hippocampus. Neuroscience. 2004; 127:69–80. [PubMed: 15219670]

Kock JH, Mecke E, Orlov OY, Reuter T, Väisänen RA, Wallgren JE. Ganglion cells in the frog retina: discriminant analysis of histological classes. Vision Res. 1989; 29:1–18. [PubMed: 2788956]

Koizumi A, Zeck G, Ben Y, Masland RH, Jakobs TC. Organotypic culture of physiologically functional adult mammalian retinas. PLoS One. 2007; 2(2):e221. [PubMed: 17311097]

Kolb H, Cuenca N, Wang HH, Dekorver L. The synaptic organization of the dopaminergic amacrine cell in the cat retina. J Neurocytol. 1990; 19:343–366. [PubMed: 2391538]

Kolb H, Linberg KA, Fisher SK. Neurons of the human retina: a Golgi study. J Comp Neurol. 1992; 318:147–187. [PubMed: 1374766]

Kong JH, Fish DR, Rockhill RL, Masland RH. Diversity of ganglion cells in the mouse retina: unsupervised morphological classification and its limits. J Comp Neurol. 2005; 489:293–310. [PubMed: 16025455]

Lavenex P, Lavenex PB, Bennett JL, Amaral DG. Postmortem changes in the neuroanatomical characteristics of the primate brain: hippocampal formation. J Comp Neurol. 2009; 512:27–51. [PubMed: 18972553]

Lin B, Martin PR, Solomon SG, Grünert U. Distribution of glycine receptor subunits on primate retinal ganglion cells: a quantitative analysis. Eur J Neurosci. 2000; 12:4155–4170. [PubMed: 11122328]

Marc RE. Mapping glutamatergic drive in the vertebrate retina with a channel-permeant organic cation. J Comp Neurol. 1999; 407:47–64. [PubMed: 10213187]

Marc, RE. Functional neuroanatomy of the retina. In: Albert, DM.; Miller, JW.; Azar, DT.; Blodi, BA., editors. Albert and Jakobiec's Principles and Practice of Ophthalmology. 3. Elsevier; 2008. p. 1565-1592.

Marc RE, Jones BW. Molecular phenotyping of retinal ganglion cells. J Neurosci. 2002; 22:413–427. [PubMed: 11784786]

Marc RE, Murry RF, Basinger SF. Pattern recognition of amino acid signatures in retinal neurons. J Neurosci. 1995; 15:5106–5129. [PubMed: 7623139]

Margo CE, Lee A. Fixation of whole eyes: the role of fixative osmolarity in the production of tissue artifact. Graefes Arch Clin Exp Ophthalmol. 1995; 233:366–370. [PubMed: 7672624]

Margolis DJ, Detwiler PB. Different mechanisms generate maintained activity in ON and OFF retinal ganglion cells. J Neurosci. 2007; 27:5994–6005. [PubMed: 17537971]

Margolis DJ, Newkirk G, Euler T, Detwiler PB. Functional stability of retinal ganglion cells after degeneration-induced changes in synaptic input. J Neurosci. 2008; 28:6526–6536. [PubMed: 18562624]

Massey SC, Miller RF. Glutamate receptors of ganglion cells in the rabbit retina: evidence for glutamate as a bipolar cell transmitter. J Physiol. 1988; 405:635–655. [PubMed: 2908248]

Mazzoni F, Novelli E, Strettoi E. Retinal ganglion cells survive and maintain normal dendritic morphology in a mouse model of inherited photoreceptor degeneration. J Neurosci. 2008; 28:14282–14292. [PubMed: 19109509]

Metz B, Kersten GF, Hoogerhout P, Brugghe HF, Timmermans HA, de Jong A, Meiring H, ten Hove J, Hennink WE, Crommelin DJ, Jiskoot W. Identification of formaldehyde-induced modifications in proteins: reactions with model peptides. J Biol Chem. 2004; 279:6235–6243. [PubMed: 14638685]

Micheva KD, Smith SJ. Array tomography: a new tool for imaging the molecular architecture and ultrastructure of neural circuits. Neuron. 2007; 55:25–36. [PubMed: 17610815]

Mirshahi M, Nicolas C, Mirshahi S, Golestaneh N, d'Hermies F, Agarwal MK. Immunochemical analysis of the sodium channel in rodent and human eye. Exp Eye Res. 1999; 69:21–32. [PubMed: 10375446]

Mittman S, Taylor WR, Copenhagen DR. Concomitant activation of two types of glutamate receptor mediates excitation of salamander retinal ganglion cells. J Physiol. 1990; 428:175–197. [PubMed: 2172521]

Muchnick N, Hibbard E. Avian retinal ganglion cells resistant to degeneration after optic nerve lesion. Exp Neurol. 1980; 68:205–216. [PubMed: 7363991]

Müller LP, Do MT, Yau KW, He S, Baldridge WH. Tracer coupling of intrinsically photosensitive retinal ganglion cells to amacrine cells in the mouse retina. J Comp Neurol. 2010; 518:4813–4824. [PubMed: 20963830]

Nelson R. Cat cones have rod input: a comparison of the response properties of cones and horizontal cell bodies in the retina of the cat. J Comp Neurol. 1977; 172:109–135. [PubMed: 838876]

Nonner W, Spalding BC, Hille B. Low intracellular pH and chemical agents slow inactivation gating in sodium channels of muscle. Nature. 1980; 284:360–363. [PubMed: 6767194]

Ogata G, Stradleigh TW, Partida GJ, Ishida AT. Dopamine and full-field illumination activate D1 and D2-D5-type receptors in adult rat retinal ganglion cells. J Comp Neurol. 2012; 520:4032–4049. [PubMed: 22678972]

Oliva AA Jr, Lam TT, Swann JW. Distally directed dendrotoxicity induced by kainic acid in hippocampal interneurons of green fluorescent protein-expressing transgenic mice. J Neurosci. 2002; 22:8052–8062. [PubMed: 12223559]

Paljärvi L, Garcia JH, Kalimo H. The efficiency of aldehyde fixation for electron microscopy: stabilization of rat brain tissue to withstand osmotic stress. Histochem J. 1979; 11:267–276. [PubMed: 110731]

Park JS, Bateman MC, Goldberg MP. Rapid alterations in dendrite morphology during sublethal hypoxia or glutamate receptor activation. Neurobiol Dis. 1996; 3:215–227. [PubMed: 8980022]

Partida GJ, Lee SC, Haft-Candell L, Nichols GS, Ishida AT. DARPP-32-like immunoreactivity in AII amacrine cells of rat retina. J Comp Neurol. 2004; 480:251–263. [PubMed: 15515184]

Perry VH, Oehler R, Cowey A. Retinal ganglion cells that project to the dorsal lateral geniculate nucleus in the macaque monkey. Neurosci. 1984; 12:1101–1123.

Peters T Jr, Ashley CA. An artefact in radioautography due to binding of free amino acids to tissues by fixatives. J Cell Biol. 1967; 33:53–60. [PubMed: 4166484]

Pourcho RG. Dopaminergic amacrine cells in the cat retina. Brain Res. 1982; 252:101–109. [PubMed: 7172014]

Pow DV, Wright LL, Vaney DI. The immunocytochemical detection of amino-acid neurotransmitters in paraformaldehyde-fixed tissues. J Neurosci Meth. 1995; 56:115–123.

Price JL, Powell TP. The morphology of the granule cells of the olfactory bulb. J Cell Sci. 1970; 7:91–123. [PubMed: 5476864]

Ramón y Cajal S. La rétine des vertébrés. La Cellule. 1893; 9:119–257.

Ramón y Cajal, S. Histology of the nervous system of man and vertebrates. Swanson, N.; Swanson, LW., translators. New York: Oxford University Press; 1899. p. 61-64.1995

Raymond ID, Vila A, Huynh UC, Brecha NC. Cyan fluorescent protein expression in ganglion and amacrine cells in a thy1-CFP transgenic mouse retina. Mol Vis. 2008; 14:1559–1574. [PubMed: 18728756]

Rivera N, Lugo N. Four retinal ganglion cell types that project to the superior colliculus in the thirteen-lined ground squirrel (Spermophilus tridecemlineatus). J Comp Neurol. 1998; 396:105–120. [PubMed: 9623890]

Rockhill RL, Daly FJ, MacNeil MA, Brown SP, Masland RH. The diversity of ganglion cells in a mammalian retina. J Neurosci. 2002; 22:3831–3843. [PubMed: 11978858]

Rodriguez AR, de Sevilla Muller LP, Brecha NA. The RNA binding protein RBPMS is a selective marker of ganglion cells in the mammalian retina. J Comp Neurol. 2014; 522:1411–1143. [PubMed: 24318667]

Rosenmund C, Stevens CF. The rate of aldehyde fixation of the exocytotic machinery in cultured hippocampal synapses. J Neurosci Meth. 1997; 76:1–5.

Sabatini DD, Bensch K, Barrnett RJ. Cytochemistry and electron microscopy. The preservation of cellular ultrastructure and enzymatic activity by aldehyde fixation. J Cell Biol. 1963; 17:19–58. [PubMed: 13975866]

Sarthy V, Hoshi H, Mills S, Dudley VJ. Characterization of green fluorescent protein-expressing retinal cells in CD 44-transgenic mice. Neurosci. 2007; 144:1087–1093.

Schaeffer SF, Raviola E. Membrane recycling in the cone cell endings of the turtle retina. J Cell Biol. 1978; 79:802–825. [PubMed: 730768]

Schmidt TM, Kofuji P. Functional and morphological differences among intrinsically photosensitive retinal ganglion cells. J Neurosci. 2009; 29:476–482. [PubMed: 19144848]

Shepherd TM, Thelwall PE, Stanisz GJ, Blackband SJ. Aldehyde fixative solutions alter the water relaxation and diffusion properties of nervous tissue. Magn Reson Med. 2009; 62:26–34. [PubMed: 19353660]

Shrager PG, Strickholm A, Macey RI. Chemical modification of crayfish axons by protein crosslinking aldehydes. J Cell Physiol. 1969; 74:91–100. [PubMed: 5799505]

Siegert S, Scherf BG, Del Punta K, Didkovsky N, Heintz N, Roska B. Genetic address book for retinal cell types. Nat Neurosci. 2009; 12:1197–1204. [PubMed: 19648912]

Slaughter MM, Miller RF. 2-amino-4-phosphonobutyric acid: a new pharmacological tool for retina research. Science. 1981; 211:182–185. [PubMed: 6255566]

Smith JE, Reese TS. Use of aldehyde fixatives to determine the rate of synaptic transmitter release. J Exp Biol. 1980; 89:19–29. [PubMed: 6110693]

Stanford LR. W-cells in the cat retina: correlated morphological and physiological evidence for two distinct classes. J Neurophysiol. 1987; 57:218–244. [PubMed: 3549992]

Stanford LR, Sherman SM. Structure/function relationships of retinal ganglion cells in the cat. Brain Res. 1984; 297:381–386. [PubMed: 6326945]

Sternberger LA, Sternberger NH. Monoclonal antibodies distinguish phosphorylated and nonphosphorylated forms of neurofilaments in situ. Proc Natl Acad Sci USA. 1983; 80:6126–6130. [PubMed: 6577472]

Stewart WW. Functional connections between cells as revealed by dye-coupling with a highly fluorescent naphthalimide tracer. Cell. 1978; 14:741–759. [PubMed: 688392]

Stone J, Holländer H. Optic nerve axon diameters measured in the cat retina: some functional considerations. Exp Brain Res. 1971; 13:498–503. [PubMed: 5137299]

Stradleigh TW, Ogata G, Partida GJ, Oi H, Greenberg KP, Krempely KS, Ishida AT. Colocalization of hyperpolarization-activated, cyclic nucleotide-gated channel subunits in rat retinal ganglion cells. J Comp Neurol. 2011; 519:2546–2573. [PubMed: 21456027]

Sun W, Li N, He S. Large-scale morphological survey of mouse retinal ganglion cells. J Comp Neurol. 2002; 451:115–126. [PubMed: 12209831]

Sutherland BW, Toews J, Kast J. Utility of formaldehyde cross-linking and mass spectrometry in the study of protein-protein interactions. J Mass Spectrom. 2008; 43:699–715. [PubMed: 18438963]

Takeuchi H, Mizuno T, Zhang G, Wang J, Kawanokuchi J, Kuno R, Suzumura A. Neuritic beading induced by activated microglia is an early feature of neuronal dysfunction toward neuronal death by inhibition of mitochondrial respiration and axonal transport. J Biol Chem. 2005; 280:10444–10454. [PubMed: 15640150]

Tartuferi F. Sulla anatomia della retina. Arch Sci Med. 1887; 11:335–358.

Tauchi M, Masland RH. The shape and arrangement of the cholinergic neurons in the rabbit retina. Proc R Soc Lond. 1984; 223B:101–119. [PubMed: 6151180]

Trommald M, Jensen V, Andersen P. Analysis of dendritic spines in rat CA1 pyramidal cells intracellularly filled with a fluorescent dye. J Comp Neurol. 1995; 353:260–274. [PubMed: 7745135]

Vaney DI. Many diverse types of retinal neurons show tracer coupling when injected with biocytin or Neurobiotin. Neurosci Lett. 1991; 125:187–190. [PubMed: 1715532]

Vaney DI, Hughes A. The rabbit optic nerve: fibre diameter spectrum, fibre count, and comparison with a retinal ganglion cell count. J Comp Neurol. 1976; 170:241–251. [PubMed: 993370]

Voigt T, Wässle H. Dopaminergic innervation of A II amacrine cells in mammalian retina. J Neurosci. 1987; 7:4115–4128. [PubMed: 2891802]

Walsh N, Fitzgibbon T, Ghosh KK. Intraretinal axon diameter: a single cell analysis in the marmoset (Callithrix jacchus). J Neurocytol. 1999; 28:989–998. [PubMed: 11054900]

Wang L, Dong J, Cull G, Fortune B, Cioffi GA. Varicosities of intraretinal ganglion cell axons in human and nonhuman primates. Invest Ophthalmol Vis Sci. 2003; 44:2–9. [PubMed: 12506048]

Watanabe M, Rodieck RW. Parasol and midget ganglion cells of the primate retina. J Comp Neurol. 1989; 289:434–454. [PubMed: 2808778]

Wayman GA, Tokumitsu H, Davare MA, Soderling TR. Analysis of CaM-kinase signaling in cells. Cell Calcium. 2011; 50:1–8. [PubMed: 21529938]

Webster HD, Ames A 3rd, Nesbett FB. A quantitative morphological study of osmotically induced swelling and shrinkage in nervous tissue. Tiss Cell. 1969; 1:201–216.

Wingate RJ, Fitzgibbon T, Thompson ID. Lucifer yellow, retrograde tracers, and fractal analysis characterise adult ferret retinal ganglion cells. J Comp Neurol. 1992; 323:449–474. [PubMed: 1430318]

Wollner DA, Catterall WA. Localization of sodium channels in axon hillocks and initial segments of retinal ganglion cells. Proc Natl Acad Sci USA. 1986; 83:8424–8428. [PubMed: 2430289]

Xu H, Tian N. Glycine receptor-mediated synaptic transmission regulates the maturation of ganglion cell synaptic connectivity. J Comp Neurol. 2008; 509:53–71. [PubMed: 18425804]

Zhan XJ, Troy JB. An efficient method that reveals both the dendrites and the soma mosaics of retinal ganglion cells. J Neurosci Meth. 1997; 72:109–116.

Zhang J, Diamond JS. Subunit- and pathway-specific localization of NMDA receptors and scaffolding proteins at ganglion cell synapses in rat retina. J Neurosci. 2009; 29:4274–4286. [PubMed: 19339621]

Zhang SX, Holmberg EG, Geddes JW. Artifactual dendritic beading in rat spinal cord induced by perfusion with cold saline and paraformaldehyde. J Neurosci Methods. 2007; 163:38–43. [PubMed: 17397933]

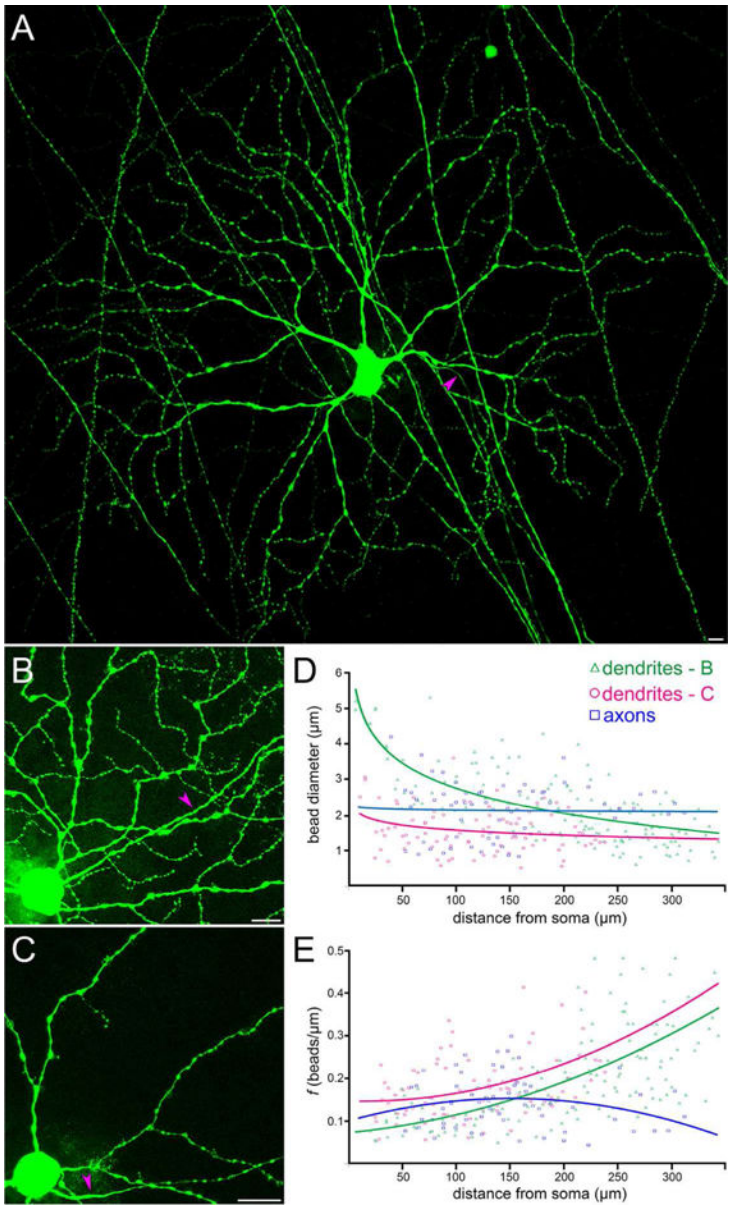

Figure 1.

GFP-expressing retinal ganglion cells preserved for 24 hr in standard FA solution (formaldehyde diluted to 4% w/v in phosphate-buffered saline). Z-projections of optical sections through the inner plexiform, ganglion cell, and nerve fiber layers of rat (A) and rabbit (B, C) retinae. GFP expression was visualized by incubating retinae in an Alexa Fluor 488-conjugated anti-GFP antibody, and assigning fluorescence from GFP and Alexa Fluor 488 to the green color channel. A: Bead-shaped varicosities in the axon and tapering, moderately branched dendrites of a single GFP-expressing cell, and in every straight, non-tapering, GFP-expressing neurite (axon or widely arborizing dendrite) projecting through the field. Beading in dendrites and axons of ganglion cells with curving and densely branching dendrites (B) and with sparsely branching, untapered dendrites (C). B and C illustrate portion of the dendritic field near soma of each cell; soma at lower left-hand corner of each

panel. An arrowhead points at the axon of each cell. Dendritic and axonal bead diameters (D), and interbead distances (E), pooled from cells in B, C, and plotted as function of distance from each soma. Scale bar in each panel is 20 μm.

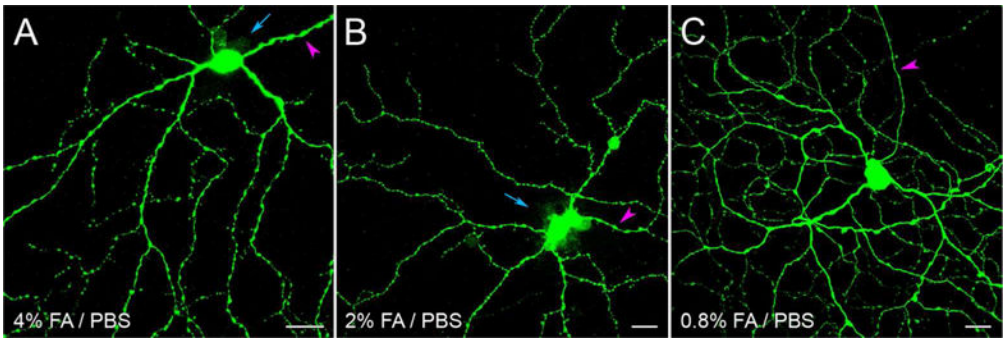

Figure 2.

GFP-expressing rabbit retinal ganglion cells preserved in standard FA solutions of various strengths. Z-projections of optical sections through the inner plexiform, ganglion cell, and nerve fiber layers of flat-mounted tissue immersed for 2 hr in FA diluted in phosphate-buffered saline to 4% w/v (A), 2% w/v (B), and 0.8% w/v (C). Bead-shaped varicosities are seen in the axons and dendrites of all cells (A–C). A fluorescent haze, possibly due to dye leakage, surrounds the soma of several cells (arrows; A, B). GFP signal amplification by Alexa Fluor 488-conjugated anti-GFP antibody, GFP and Alexa Fluor 488 fluorescence display, arrowheads, and 20-μm calibration marks as in Figure 1.

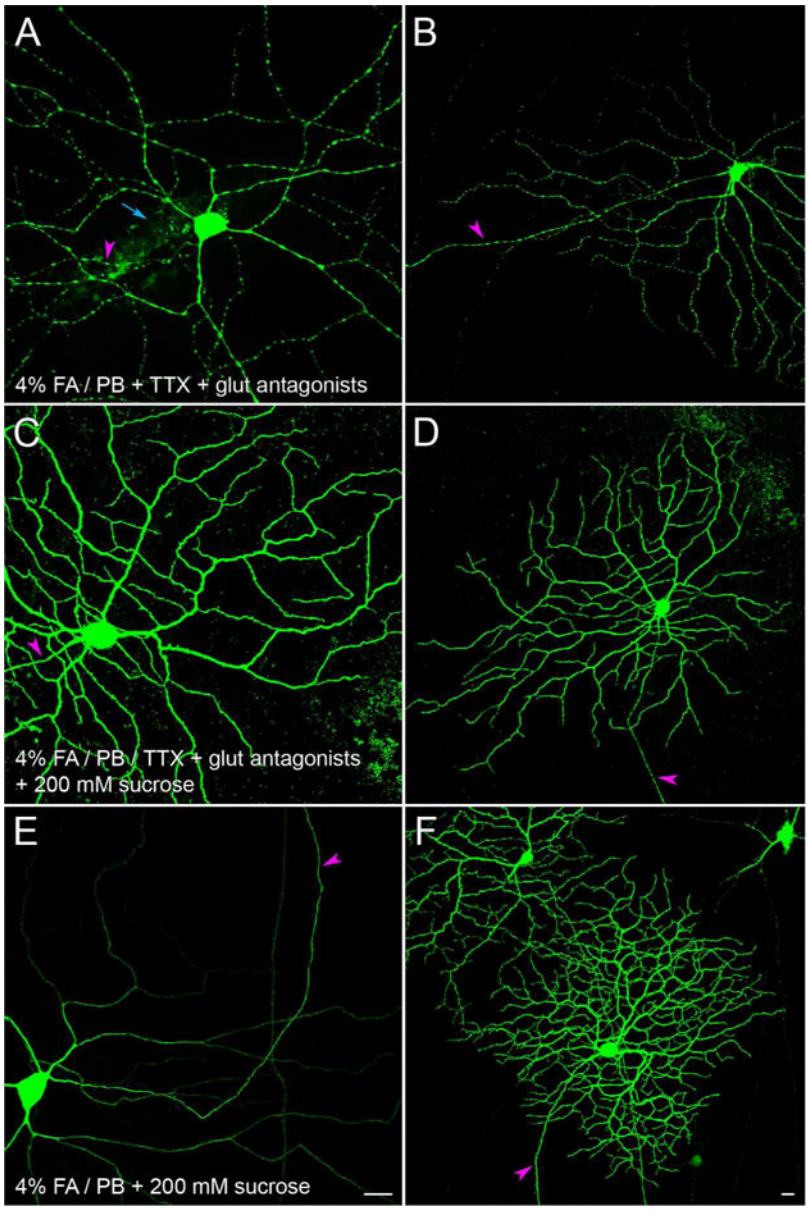

Figure 3.

GFP-expressing rabbit retinal ganglion cells following immersion in three variants of low-Na+ fixative. A,B: LSA fixative (4% FA diluted in Sørensen's phosphate buffer, supplemented with glutamate receptor antagonists and TTX). C,D: LSA fixative supplemented with sucrose. E,F: protectant fixative (4% FA diluted in Sørensen's phosphate buffer, supplemented with sucrose). Fixation time was 24 hr for A–D, 2 hr for E–F. Each panel (A–F) shows a z-projection of optical sections through the inner plexiform, ganglion cell, and nerve fiber layers. A,C,E imaged to view details of dendrites and axons. B,D,F imaged to capture larger portions of the dendritic fields and axons. GFP signal amplification by Alexa Fluor 488-conjugated anti-GFP antibody, GFP and Alexa Fluor 488 fluorescence display, arrowheads, and 20-μm calibration marks as in Figure 1.

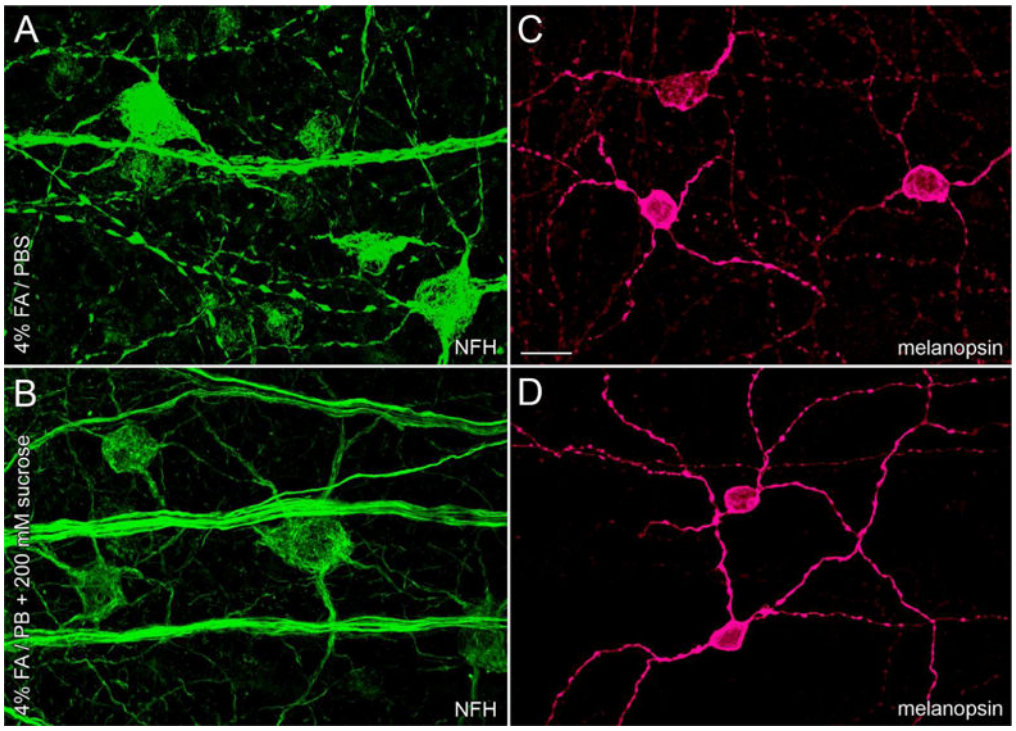

Figure 4.

Inner retinal neurons immunostained for neurofilament H (NFH) and melanopsin. Rat retinae were immersion-fixed in FA diluted in either PBS (A,C) or PB supplemented with 200 mM sucrose (B,D). Each panel (A–D) shows a z-projection of optical sections through the inner plexiform, ganglion cell, and nerve fiber layers. A,B: The anti-NFH antibody stains large somata, their tapering dendrites, and axon fascicles. C,D: The anti-melanopsin antibody stains smaller somata with sparse, non-tapering dendrites. Calibration mark in B is 20 μm and applies to all panels.

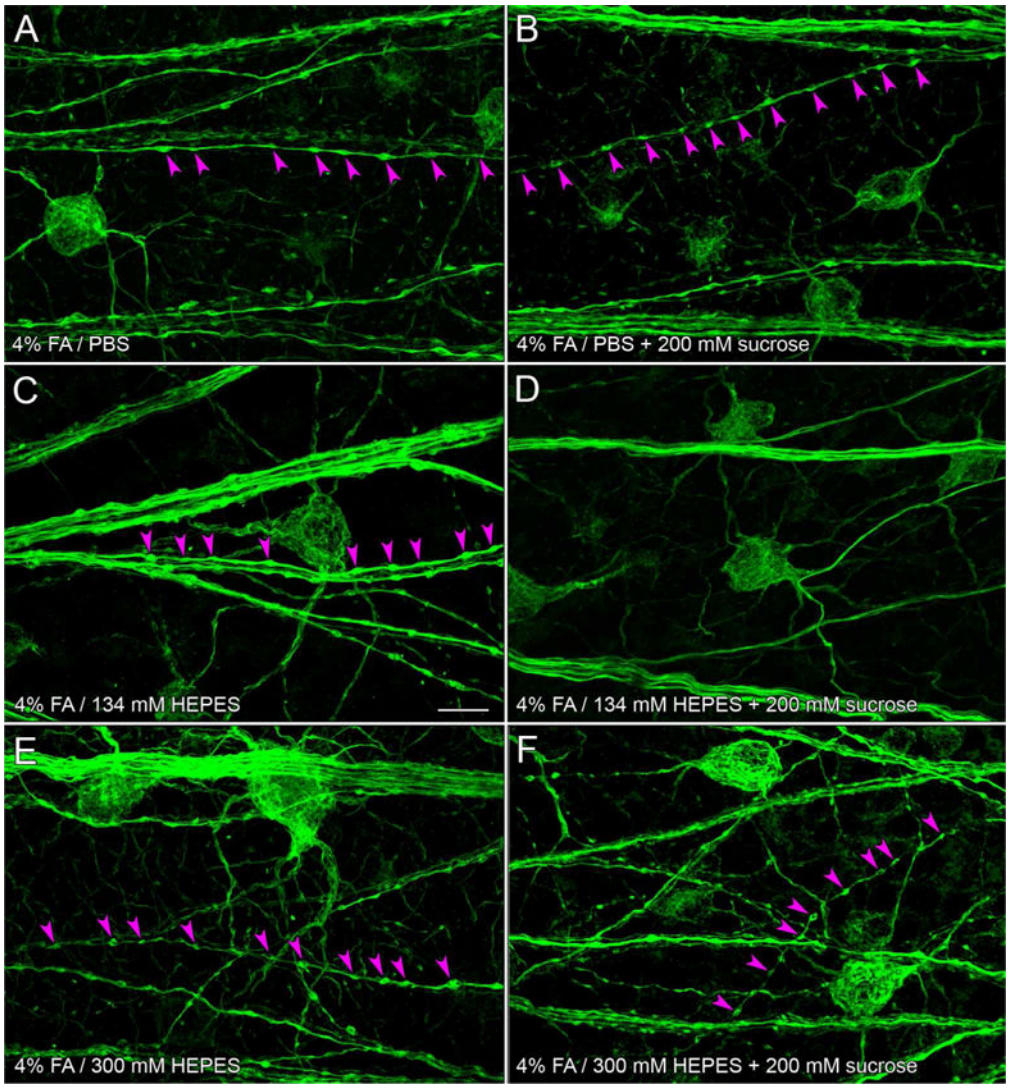

Figure 5.

NFH-like immunoreactivity in rat retinal ganglion cells following immersion-fixation in FA diluted to 4% in either PBS or HEPES, and each fixative supplemented with 200 mM sucrose, as labeled. Each panel (A–F) shows a z-projection of optical sections through the inner plexiform, ganglion cell, and nerve fiber layers. Arrowheads point to bead-like varicosities in one exemplar axonal fiber per field (A–C, E–F). All immunostained dendrites and axons are bead-free in D. Calibration mark in C is 20 μm and applies to all fields.

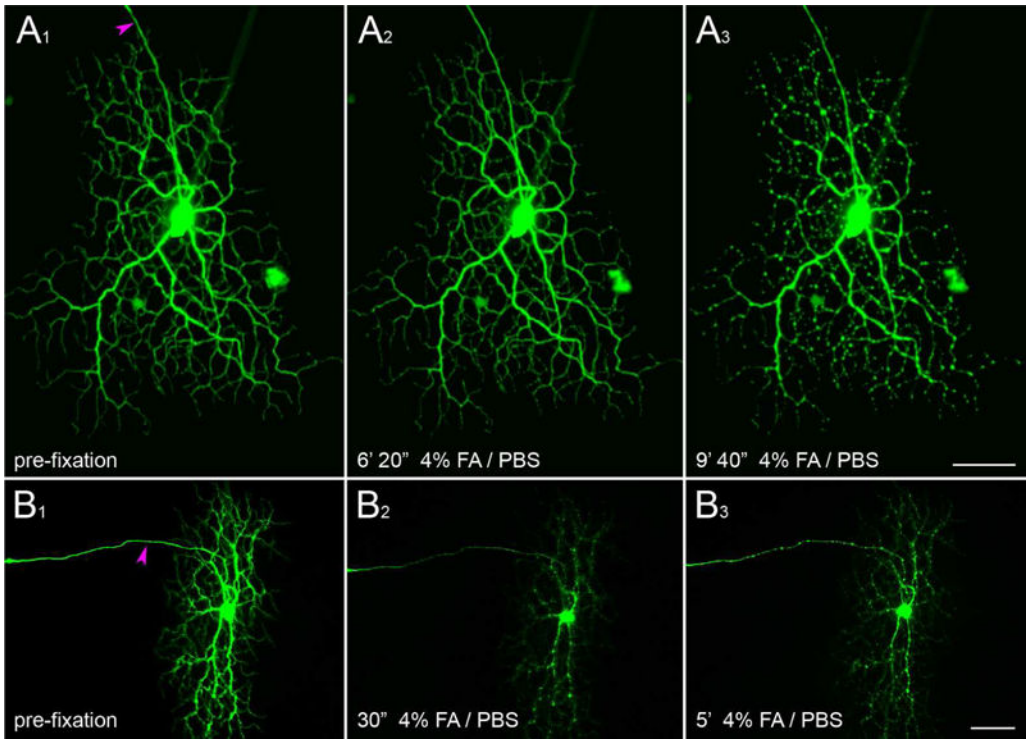

Figure 6.

Still images taken from time-lapse videos of GFP-expressing rat retinal ganglion cells during preservation in standard FA. Cells were imaged before the addition of fixative solution (A_1, B_1) and at regular intervals after the addition of FA. Arrowheads point at axons (A_1, B_1). Calibration mark in A_3 is 100 μm and applies to A_1–A_3. Calibration mark in B_3 is 100 μm and applies to B_1–B_3.

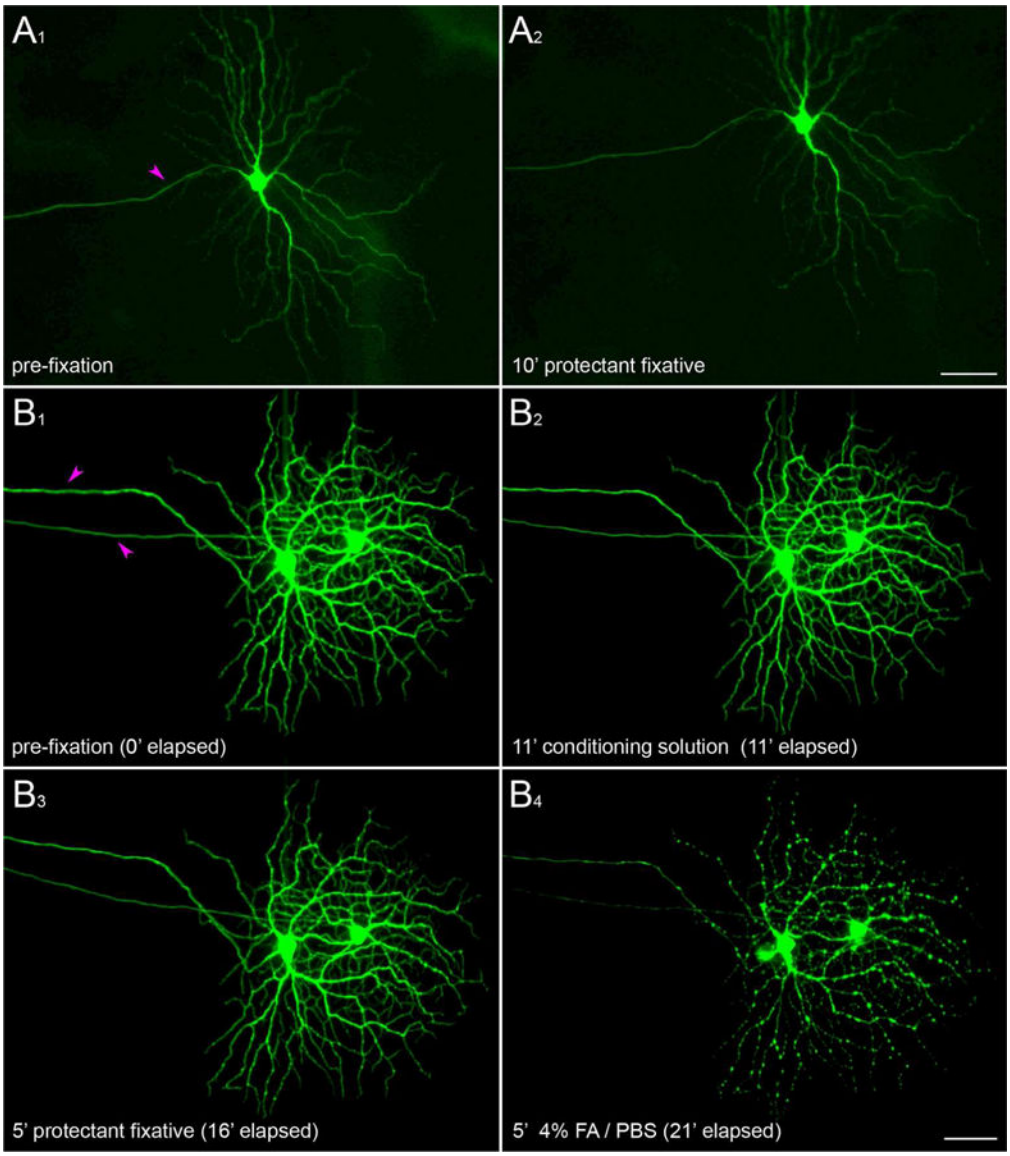

Figure 7.

Still images taken from time-lapse videos of GFP-expressing rat retinal ganglion cells during preservation in protectant fixative solutions. Cells (n = 1 in A, n = 2 in B) were imaged before the addition of protectant fixative solutions (A_1, B_1) and at regular intervals after the addition of fixatives. A: Cell exhibited no noticeable beads or bead formation before superfusion with fixative or while in protectant solution. B: Cells exhibited relatively few beads before superfusion with fixative protectant solution and no noticeable increase in beads after 5 min in protectant solution. B_4: Beading formed throughout the dendritic arbors, and in axons, within 5 min of immersion in standard FA fixative. Arrowheads point at axons (A_1, B_1). Calibration mark in A_2 is 100 μm and applies to A_1–A_2. Scale bar in B_4 is 100 μm and applies to B_1–B_4.

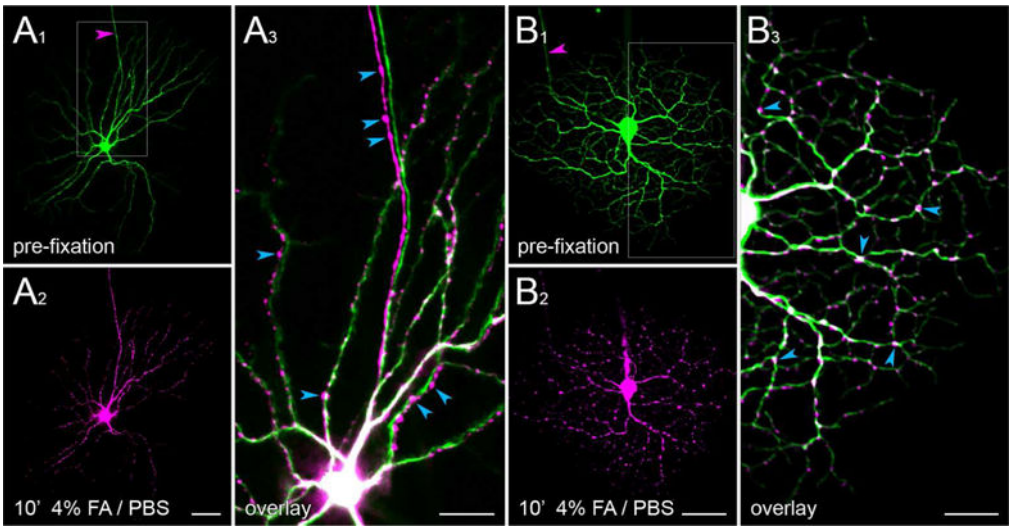

Figure 8.

Still images taken from time-lapse videos of GFP-expressing rat retinal ganglion cells during immersion in standard FA. Cells were imaged before the addition of fixative solution (A_1, B_1) and 10 min after the addition of fixative (A_2, B_2). High magnification display of fields outlined in A_1, B_1 from each cell before and after the addition of fixative were superimposed to compare neurite contour in dendrites (A_3, B_3) and an axon (A_3). Fluorescent signal from pre-fixation and post-fixation images were false-colored green and magenta, respectively. Regions of overlapping signal appear white. Arrowheads point at axons (A_1, B_1). Calibration mark in A_2 is 100 μm and applies to A_1–A_2. Calibration mark in B_2 is 100 μm and applies to B_1–B_2. Calibration marks in A_3 and B_3 are each 50 μm.

Table 1

Summary of Fixative Buffers

Buffer	Components	Mean Osmolality (SEM)
standard	potassium phosphate monobasic (1.06 mM) sodium phosphate dibasic (2.97 mM) sodium chloride (155.17 mM)	301 mmol/kg (0.88)
LS	sodium phosphate monobasic (33.5 mM) sodium phosphate dibasic (33.5 mM) TTX (1 μM)	147 mmol/kg (0.33)
LSA	sodium phosphate monobasic (33.5 mM) sodium phosphate dibasic (33.5 mM) TTX (1 μM); RS-CPP (10 μM); CNQX (10 μM); L-AP4 (20 μM)	147 mmol/kg (0.39)
protectant	sodium phosphate monobasic (33.5 mM) sodium phosphate dibasic (33.5 mM) sucrose (200 mM)	347 mmol/kg (2.33)
HEPES	HEPES (134 or 300 mM)	203 mmol/kg (0.21) 479 mmol/kg (1.15)

LS: low-sodium Sørensen's phosphate buffer with TTX; LSA: low-sodium Sørensen's buffer with TTX and glutamate receptor antagonists; RS-CPP: (RS)-3-(2-carboxypiperazin-4-yl)-propyl-1-phosphonic acid; CNQX: 6-cyano-7-nitroquinoxaline-2,3-dione; TTX: tetrodotoxin; HEPES: 4-(2-hydroxyethyl)-1-piperazineethanesulfonic acid; L-AP4: L-(+)-2-amino-4-phosphonobutyric acid

Table 2

Summary of Primary Antibodies

Antibody	Immunogen	Source	Species	Concentration
anti-GFP, RRID:AB_10058149	green fluorescent protein, *Aequorea victoria*	Life Technologies (A21311)	rabbit IgG, polyclonal	2 μg/mL
anti-melanopsin, RRID:AB_2156044	synthetic peptide corresponding to residues 1–19 of rat melanopsin	Thermo-Fisher (PA1-780)	rabbit IgG, polyclonal	0.3 μg/mL
anti-NFH, RRID:AB_1566483	non-phosphorylated epitope on heavy molecular weight neurofilament H (200 kD)	Abcam (AB73273)	mouse IgG1, clone SMI-32	0.3 μg/mL